CD44 targeted delivery of siRNA by using HA-decorated nanotechnologies for KRAS silencing in cancer treatment

A Tirella[1,2,*], K Kloc-Muniak[3], L Good[3,4], J Ridden[3], M Ashford[5], S Puri[5], N Tirelli[1,2,6]

[1] Division of Pharmacy and Optometry, Faculty of Biology, Medicine and Health, University of Manchester, Manchester Academic Health Science Centre, Oxford Road, Manchester, M13 9PL, United Kingdom
[2] NorthWest Centre for Advanced Drug Delivery (NoWCADD), Faculty of Biology, Medicine and Health, University of Manchester, Oxford Road, Manchester, M13 9PT, United Kingdom
[3] Tecrea Ltd. 2 Royal College Street, London, NW1 0NH, UK
[4] Department of Pathology and Population Sciences, Royal Veterinary College, Royal College Street, London, NW1 0TU, UK
[5] Advanced Drug Delivery, Pharmaceutical Sciences, IMED Biotech Unit, AstraZeneca, Cambridge, UK
[6] Laboratory of Polymers and Biomaterials, Fondazione Istituto Italiano di Tecnologia, 16163 Genova, Italy
* Corresponding author: annalisa.tirella@manchester.ac.uk, Division of Pharmacy and Optometry, Stopford Building, FBMH, University of Manchester, Oxford Road, Manchester, M13 9PT, phone +44 (0) 161 275 4769

Keywords: Hyaluronan, CD44, polymer therapeutics, siRNA, KRAS

Abstract

KRAS is a small GTPase that regulates cell proliferation and survival. In tumors, the KRAS gene is mutated, and leading to unregulated tumor growth. Despite the recognized importance of KRAS in cancer, attempts to develop small molecule inhibitors have proved unsuccessful. An alternative strategy is gene silencing and the use of small nucleic acid sequences (e.g. siRNA, shRNA), has been reported to successfully downregulate KRAS. In this study we developed ternary nanocomplexes to deliver an anti-KRAS siRNA to colorectal cancer cells, exploiting the interaction of hyaluronic acid (HA) with CD44 as a means to achieve selective targeting of CD44-positive cancer cells. Two different polycations, poly(hexamethylene biguanide) and chitosan, were complexed with siRNA and coated with HA. Physico-chemical properties and stability of nanoparticles were characterized, including size, surface charge, and degree of siRNA protection. We demonstrate nanoparticle internalization (flow cytometry), siRNA cytosolic release (confocal microscopy) and KRAS silencing (RT-qPCR) in $CD44^{+}/KRAS^{+}$ colorectal cancer cell line, HCT-116. Further we demonstrate that the uptake of HA-decorated nanoparticles in cancer cells is higher when co-cultured with fibroblasts.

Graphical abstract

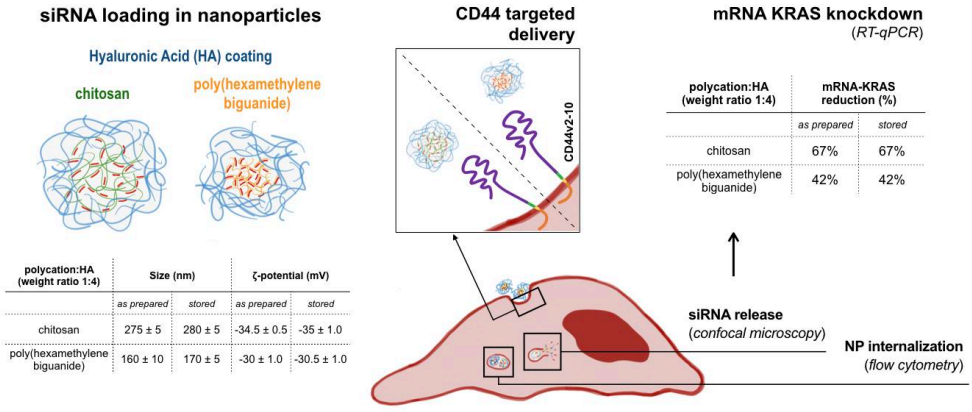

polycation:HA (weight ratio 1:4)	Size (nm)		ζ-potential (mV)	
	as prepared	*stored*	*as prepared*	*stored*
chitosan	275 ± 5	280 ± 5	-34.5 ± 0.5	-35 ± 1.0
poly(hexamethylene biguanide)	160 ± 10	170 ± 5	-30 ± 1.0	-30.5 ± 1.0

polycation:HA (weight ratio 1:4)	mRNA-KRAS reduction (%)	
	as prepared	*stored*
chitosan	67%	67%
poly(hexamethylene biguanide)	42%	42%

1. Introduction

KRAS is a small GTPase involved in the regulation of numerous cellular processes, including growth, proliferation, survival and other aspects of cellular biology accordingly to its active/inactive state (Ellis and Clark, 2000). KRAS mutations impair the ability of the KRAS protein to switch between states, hence mutated KRAS acquires oncogenic properties; such mutations are observed in approximately 30% of tumors. In particular, pancreatic and colorectal cancers (Cox et al., 2014; Ross et al., 2017; Stephen et al., 2014), are involved in tumor initiation and maintenance (Chin et al., 1999; Collins et al., 2012; Zhang et al., 2006) and are associated with poor prognosis and increased resistance to treatment, including targeted therapies (e.g. EGFR-TKIs (Überall et al., 2008)). Therefore, it is not surprising that KRAS is considered an attractive target, but unfortunately an elusive one, since its intracellular location (Blasco et al., 2011) and very low concentration make its selective inhibition very challenging. To date, probably the most successful approach has employed farnesyl transferase inhibitors (KRAS activation requires post-translational farnesylation), and the use of small molecules to block mutant KRAS and RAS family protein and their downstream effectors have been developed or are under clinical trial studies (Appels et al., 2005; Asati et al., 2017; Shin et al., 2018; Wang et al., 2013). Alternatively, small interfering RNA (siRNA) has been employed to target KRAS (Collisson et al., 2012; Hatzivassiliou et al., 2013; Kamerkar et al., 2017; Ross et al., 2017), with some systems translated to up to phase III trials for the intra-tumoral delivery of siRNA to downregulate KRAS, and reduce KRAS activity in pancreatic tumors (Zorde Khvalevsky et al., 2013).

Recently, it has been shown that the regulation of KRAS-mediated signaling in lung adenocarcinoma is strongly linked to CD44 expression (Zhao et al., 2013): interestingly, CD44 is both a diagnostic/prognostic marker [16] and a targetable internalization receptor [15], hence this association may open the way to more selective KRAS-targeted treatments. In both its standard and higher molecular weight variant isoforms (CD44v2-v10), CD44 has a major role as a cell surface receptor for hyaluronic acid (HA) (Mattheolabakis et al., 2015; Ponta et al., 2003) responsible for both its recognition, binding and internalization (Culty et

al., 1992). In tumors, CD44 is often expressed as its higher molecular weight variant isoforms, known to alter cellular behavior and signaling pathways (Culty et al., 1992; Misra et al., 2008). The variant isoform CD44v6 is of particular interest: it is not only expressed when tumor associated fibroblasts are activated, but also triggers receptor kinase activities suggesting again a correlation between CD44 and KRAS in adenocarcinomas (Kim et al., 1994; Misra et al., 2011). Unsurprisingly, HA has been widely employed in the context of CD44-targeting therapies, e.g. to improve water solubility or overcome drug resistance (Auzenne et al., 2007; Coradini et al., 1999; Luo et al., 2002; Yi Luo et al., 2000), with some successful cases currently in clinical trials (Bassi et al., 2011; Rios de la Rosa et al., 2018). We are specifically interested in HA-presenting colloidal carriers, which include liposomes (Surace et al., 2009), solid nanoparticles (Li et al., 2013; Ma et al., 2012; Yu et al., 2013), or self-assembly nano-systems (Ganesh et al., 2013; Janes et al., 2001; Lallana et al., 2017). These systems in principle, combine CD44 targeting and CD44-mediated internalization with the Enhanced Permeation and Retention (EPR) effect (Stylianopoulos and Jain, 2015), which can further help the selectivity of a targeted therapy.

Optimal therapeutic strategies should specifically target the mutated KRAS gene and have minimal systemic toxicity. To improve the selectivity and delivery of anticancer therapeutics, an effective strategy may require target-ligand interactions and formulation of nanoparticles able to promote internalization and cargo release at the desired intracellular site to effectively address the clinical translation aspects (Birzele et al., 2015; Karousou et al., 2017; Rios de la Rosa et al., 2017a). One strategy that our group and others have explored over the past decade is the use of HA-decorated nanoparticles in order to deliver nucleic acid via CD44-HA interactions. HA provides stability, low protein adsorption and CD44-targeting to the nanoparticles, which include also a polycation that binds both to HA and the payload (‘glueing’ together the carrier) and would then be responsible for endosomal disruption typically through the ‘proton sponge’ mechanism (Almalik et al., 2013b; Deng et al., 2014; Lallana et al., 2017; Parajó et al., 2010). A critical attribute for such systems is indeed the nature of the polycation, which impacts dramatically on the transfection efficiency. Chitosan;

for example, requires a careful optimization of molecular weight and degree of acetylation to achieve effective siRNA delivery (Lallana et al., 2017). In the context of achieving a CD44-mediated KRAS silencing therapy, we here investigated the influence of two main descriptors of the polycation performance, i.e. size and charge density. To enable this, we prepared a range of nanoparticles employing high molecular weight chitosan and low molecular weight poly(hexamethylene biguanide), commercially known as Nanocin (Chindera et al., 2016). The two respectively act as a very large, poorly charged polycation, and as a very small, densely charged one. Nanoparticles with anti-KRAS siRNA were obtained via combination of chitosan or Nanocin and HA coating and compared investigating nanoparticles: stability/efficacy in the presence of RNases and after storage, ability to deliver siRNA in $CD44^{+}$ tumor cells (colorectal cancer cell line HCT-116), and reduction in KRAS expression. We further investigated the potential of selective delivery of HA-decorated nanoparticles to cancer cells (HCT-116: $CD44^{+}$, $CD44v6^{high}$) when the latter were co-cultured with $CD44^{low}$ fibroblasts (HDFa).

2. Materials and Methods

2.1 Nanoparticles and siRNA loading

2.1.1 Material preparation. All materials used in this study were handled under RNase free conditions: solutions were prepared with nuclease-free solvents, and materials were either purchased RNase free or made RNase free by sequential washing with RNaseZap® RNase Decontamination Solution (Ambion, LifeTechnologies, UK), 70% v/v EtOH in water, and finally sterile nuclease-free water (Ambion, Life Technologies, UK) prior to use. Both polymeric nanotechnologies were manufactured under controlled mixing conditions using round-bottom vials (2 mL Safe-Lock Tubes, 2 mL, round bottom, PCR clean, Eppendorf, UK) and magnetic stirring bars (micro 7 mm × 2 mm, Fisher Scientific, UK). Polycations: Chitosan from crab shells with viscosity average molecular weight of 656 kDa (Almalik et al., 2013a), was purchased from Sigma Aldrich (Basingstoke, UK; Product code: 51009219, Lot#WE44069811), and purified prior to use as described elsewhere (Mao et al., 2004).

Poly(hexamethylene biguanide), also known as polyhexanide and as Nanocin, with average molecular weight approximately of 3.2 kDa (www.tecrea.com) was prepared as a sterile solution with a concentration of 1 mg/mL in RNase free water. Hyaluronic acid (HA) with weight average molecular weight of 183 kDa (GPC with SLS, viscometer and RI detectors) was purchased from Contipro (Czech Republic). Selected anti-KRAS sequence (siRNA): 1 mg/mL stock solutions of siRNA were prepared in RNase-free water for both L3-siRNA (sense 5'-3': GGACUCUGAAGAUGUACCU[dT][dT] 21nt, standard purification, Sigma-Aldrich, UK) and DY547-labeled L3-siRNA (5'-DY547 GGACUCUGAAGAUGUACCU-3', Dharmacon, UK). Polymeric solutions used for the manufacturing of nanoparticles were prepared as follows. Chitosan was dissolved overnight at a concentration of 0.69 mg/mL in 4.6 mM HCl (aq) in nuclease-free water and then pH adjusted to 5 by adding nuclease-free 0.1 M NaOH (aq). Chitosan solution was sterile filtered using 0.45 μm PDVF syringe filters. Nanocin sterile solution was diluted to 0.69 mg/mL with RNase free sterile water. HA was dissolved overnight in RNase free water at a concentration of 1.5 mg/mL, and then the pH was adjusted to 5 by adding nuclease-free 0.1 M HCl (aq). HA solution was sterile filtered using 0.22 μm PES syringe filters. HA solutions with different concentrations were obtained by diluting the 1.5 mg/mL solution in nuclease-free water. Sterile siRNA solutions were prepared at the desired concentration by diluting the 100 μM stock solution (aq) with RNase free and sterile water and stored at -20°C until use.

2.1.2 Preparation of nanoparticles. HA-coated nanoparticles were prepared with a concentration of 1 mg/mL in water, using a procedure similar to the one already described by Lallana et al. (Lallana et al., 2017) for the preparation of RNA-loaded HA/chitosan ternary complexes. In a typical procedure, a given volume of the 0.69 mg/mL polycation (chitosan or Nanocin) solution was gently pipetted over the same volume of the siRNA solution (with concentration adjusted the targeted % wt. loading) under magnetic stirring (1,000 rpm, 25°C). After 20 min, the polycation/siRNA complex dispersion was gently pipetted to the same volume of a 1.5 mg/mL HA solution under magnetic stirring (1,000 rpm, 25°C). The final

mixture was stirred for further 30 min to obtain siRNA-loaded nanoparticle formulations of ca. 1 mg/mL (calculated from the nanoparticle polyelectrolyte feed ratio). A typical loading of 2.3% wt. siRNA (compared to the polycation) was used for nanoparticle characterization and cell culture experiments. Please note that from now the term nanoparticles (NP) refers to both HA-coated Nanocin or chitosan nanoparticles.

2.1.3 Preparation of nanoparticles varying polycation:HA ratio. NP were prepared varying polycation:HA ratio to identify the optimal formulation in terms of size and ζ potential. NP were prepared using HA solutions with the following concentration (polycation:HA ratio): 0.375 mg/mL (1:1), 0.75 mg/mL (1:2), 1.125 mg/mL (1:3) and 1.5 mg/mL (1:4). For uncoated NP (1:0 ratio), RNase free water (pH adjusted to 5) was used. NP were prepared using the same procedure described above (Section 2.1.2). Briefly, the polycation/siRNA complex dispersion was pipetted in an equivalent volume of HA at different concentrations to vary the polycation:HA weight ratio. Note that in this case the final concentration of NP varies from 0.35 mg/mL (1:0) to 1 mg/mL (1:4).

2.1.4 Preparation of nanoparticles varying siRNA loading. NP were prepared by loading different amount of siRNA, i.e. 2.3% wt., 25% wt. weight ratio compared to polycation content. siRNA solutions were prepared in RNase free and sterile water at different concentrations, 0.016 mg/mL (2.3% wt.) and 0.172 mg/mL (25% wt.). NP were prepared as described above (Section 2.1.2).

2.2 Nanoparticle characterization

2.2.1 Dynamic Light Scattering (DLS). NP (1mg/mL in water) hydrodynamic diameter (Z-average size), size polydispersity (PDI), and ζ potential were measured at 25°C (pre-equilibration for 2 min; 1 mg/mL) using a Zetasizer Nano ZS (model ZEN3600, Malvern Instruments Ltd., UK) equipped with a solid state HeNe laser (λ = 633 nm) at a scattering

angle of 173°. Size distributions were calculated by applying the general-purpose algorithm and are presented as the average of the Z-average values of three independent samples.

2.2.2 Payload protection against RNAse. NP (1mg/mL in water) used in this study were prepared by loading an amount of siRNA corresponding to 25%wt. of the polycation (13 μM siRNA solution) -/+ HA coating. Briefly, 50 μL of NP were incubated with 50 μL of a solution of RNase I (AM2294, Ambion, Thermofisher Scientific) (15 mM Tris buffer, 0.3 M NaCl, pH 7.0) at a concentration of 0, 0.33, and 3.33 U (corresponding to 0, 0.1, 1 and 10 U of RNase I/mL, respectively). Samples were incubated at 37°C for 30 min. The nuclease reaction was then quenched with the addition of 7.6 μL of 1.0% SDS (aq). Afterward, 3 μL of chitosanase (0.066 U/μL, 50 mM acetate buffer, pH 5.0) was added to the mixture, and the enzymatic reaction was allowed to occur for 3 h at 37°C. Finally, 4.7 μL of a solution of heparin (80 mg/mL in RNase-free water; corresponding approximately to a negative/positive charge molar ratio of of 250) was added. The resulting mixture was incubated overnight at 25°C. After centrifugation (13,000 rpm, 30 min), the nucleic acid released in solution was quantified using polyacrylamide gel electrophoresis (siRNA; 18-well/30 μL, 15% Criterion TBE-Urea Gel, Biorad; 70 min, 120 V). Gels were finally incubated for 30 min in a 1X GelRedTM solution and imaged using a UV trans-illuminator (Biorad).

2.2.3 Nanoparticle stability. NP were stored at 4°C for one week and then tested to check variations in size, surface charge and efficacy (for silencing experiments details refer to section 2.7).

2.3 Cell culture and CD44 characterization

2.3.1 General cell culture. All cell culture experiments and following procedures were performed at the University of Manchester (UK), unless otherwise specified. The human colorectal carcinoma cell line HCT-116 (CCL-247) was purchased from ATCC (Manassas, VA, USA) and the adult human dermal fibroblast (HDFa, #C0135C) cell line was purchased

from Thermo-Fisher Scientific (UK). Cells were cultured in a humidified 5% (v/v) CO_2 air atmosphere at 37°C in complete medium, cell culture growth media were supplemented with 10% (v/v) fetal bovine serum (FBS, F7524), 2 mM L-glutamine (G7513) and 1% (v/v) penicillin−streptomycin (P4333). McCoy's 5A medium (M8403) and DMEM (D5671) were used for HCT-116 and HDFa, respectively. Please note that cells were regularly tested for mycoplasma and used at passage numbers below 20, and that all cell culture products were purchased from Sigma- Aldrich (Gillingham, UK).

2.3.2 CD44 expression: flow cytometry. Cells were grown in T-75 flasks until reaching ~70% confluency and harvested using pre-warmed Enzyme-Free, Phosphate Buffer solution (PBS)-based Cell Dissociation Buffer (#13151-014, Gibco®/Invitrogen, UK). Individual cell samples were prepared in 1.5 mL Eppendorf tubes by suspending approximately 100,000 viable cells in 100 µL Fluorescence-Activated Cell Sorting (FACS) buffer (PBS, 5% (v/v) FBS, 0.1% (m/v) NaN_3) and stained for 30 min at room temperature with the primary antibody mouse anti-human CD44 (1:100) (156-3C11, Cell Signalling Technology, UK) or IgG1/IgG2 control (1:10) (AbD Serotec, UK). Excess primary antibody was removed by centrifugation and cells were incubated for further 30 min at room temperature with the secondary antibody: goat anti-mouse IgG H&L, AlexaFluor®647-conjugated (1:2000) (ab150115, Abcam, UK). The expression of total CD44 (CD44pan) was recorded for 10,000 live, individual cells using a BD LSRFortessa cytometer (BD Bioscience, San Jose CA, USA) equipped with the FACSDiva software (v8.0.1). Data were analyzed with FlowJo (vX.0.7, Tree Star, Ashland, OR, USA) after gating live cells in the FSC/SSC window and cell singlets in the FSC-H/FSC-A window, respectively. The median fluorescence intensity (MFI) of the isotype control for each cell line was used to calculate the MFI fold change for each marker.

2.3.3 CD44 expression: immunofluorescence staining. HCT-116 cells were plated in Ibidi µ-slide (prod.no. 80826, Ibidi®, Germany) at 70% of confluency (approx. 8,000 cells, 37°C, 5% CO_2) and left adhere overnight. Live cells were then stained with the following primary

antibodies: i) mouse anti-human CD44 (1:100) (156-3C11, Cell Signaling Technology, UK), ii) mouse anti-human CD44v3 (1:20) (Clone #3G5, R&D Systems, UK), iii) mouse anti-human CD44v6 (1:20) (Clone #2F10, R&D Systems, UK); hence detecting only membrane bound CD44. Briefly, cells were washed with PBS, incubated with mouse anti-human CD44 primary antibody solutions diluted in 1% (w/v) BSA/PBS on ice for 30 min, gently washed with PBS, and incubated with 1:250 goat anti-mouse IgG H&L, AlexaFluor®488-conjugated (ab150117, Abcam, UK) on ice for additional 30 min. Cells were finally washed with PBS (twice), fixed with 4% PFA solution (5 min, RT), washed with PBS and stored in 1 mg/mL ascorbic acid solution in PBS at 4°C in the dark until further use.

2.4 Nanoparticle internalization

NP (0.125 mg/mL, final concentration) for cell experiments were prepared in complete cell growth medium as follows, a final siRNA concentration of 40 nM (0.5 µg/mL) was obtained. HA-coated chitosan NP (1 mg/mL in water) were diluted after preparation to a concentration of 250 µg/mL with sterile and nuclease-free water. The final concentration of 125 µg/mL used for cell culture experiment was obtained by addition of an equal volume of two-fold cell culture medium (refer to Supporting Information SI.1 for the preparation of concentrated cell culture medium). Nanocin/HA NP (1 mg/mL) were diluted after preparation by adding 11.6 µL of nanoparticles to complete cell culture media to a final volume of 1 mL. Note that kinetic of internalization studies were performed loading DY547-siRNA (L3 sequence: 5'-DY547 GGACUCUGAAGAUGUACCU-3'; Dharmacon, UK) in NP (i.e. DY547-NP).

2.4.1 Quantification of nanoparticle internalization: flow cytometry. Cells were plated in Costar tissue culture polystyrene (TCP) 12-well plates with flat bottom (#3513, Corning, UK) and incubated (37°C, 5% CO_2) with 125 µg/mL DY547-NP for specific time points: 4, 12, and 24 h. Untreated cells were used as a negative control. After each incubation time, nanoparticle-containing medium was removed, cells were washed with PBS (n=3) and detached using Trypsin-EDTA solution (#59417C, Sigma-Aldrich, UK) for 10 min at room

temperature. Trypsin was used to remove any residual membrane-bound nanoparticle, enabling the detection of internalized nanoparticles exclusively (Rios de la Rosa et al., 2017b). Cells were pelleted (1000 rpm, 5 min, 25°C) and re-suspended in 400 µL PBS. The internalization of DY547-NP was determined on 10,000 individual and live cells with the BD LSRFortessa cytometer (BD Bioscience, San Jose CA, USA) equipped with the FACSDiva software (v8.0.1). Data were analyzed with FlowJo (vX.0.7, Tree Star, Ashland, OR, USA) after gating single and live events in the FSC-A/FSC-H and FSC/SSC windows, respectively. Untreated cells were used as autofluorescence control in order to calculate the median fluorescence intensity (MFI) fold change over time, as well as the percentage of positive events for each cell line.

2.4.2 Nanoparticle late endosome/lysosome escape: confocal microscopy. HCT-116 cells were plated in Ibidi µ-slide (prod.no. 80826, Ibidi®, Germany) at 70% of confluency and left adhere overnight (37°C, 5% CO_2). A volume of 100 µL of DY547-NP (125 µg/mL in complete cell culture media) was added to each well and cells were incubated for 1 h (37°C, 5% CO_2), DY547-NP containing medium was then removed, cells were gently washed with PBS (n=2) and co-incubated with 100 nM Lysotracker Green (L7526, Invitrogen, Thermo Fisher, UK) and 1 µM Hoechst (33342, Invitrogen, Thermo Fisher, UK) solution (37°C, 5% CO_2, 10 min). Cells were finally gently washed with PBS (n=2), kept in 1 mg/mL ascorbic acid solution in PBS and immediately imaged with laser scanning confocal microscope.

2.4.3 Nanoparticle uptake and role of HA-coating: confocal microscopy. HCT-116 cells were plated in Ibidi µ-slide (prod.no. 80826, Ibidi®, Germany) at 70% of confluency and left adhere overnight (37°C, 5% CO_2). HA-coated and uncoated DY547-NP (125 µg/mL in complete cell culture media) were used. A volume of 100 µL of DY547-NP was added to each well and cells were incubated for 24 h (37°C, 5% CO_2), nanoparticle-containing medium was then removed, cells were gently washed with PBS (n=2), incubated (37°C, 5% CO_2, 10 min) with 1 µM Hoechst solution in PBS (33342, Invitrogen, Thermo Fisher, UK), cells were

gently washed with PBS (n=2), kept in 1 mg/mL ascorbic acid solution in PBS and immediately imaged with laser scanning confocal microscope.

2.5 Co-culture experiments: HCT-116 and fibroblasts

Co-culture experiments were performed using TCP 6-well plates with flat bottom (Prod. No. 3513, Corning, UK). HCT-116 cells were seeded at a density of 10,000 cells/cm^2 on the bottom of the wells, whereas fibroblasts (HDFa) were seeded on transwell inserts (MW6 Transwell Inserts, 0.4μm PET Membrane, Corning, UK) at a density of 10,000 cells/cm^2. Cells were left adhere for 12 h in separate multi-well plates (37°C, 5% CO_2), then inserts culturing HDFa cells were transferred to the 6-well plates culturing cancer cells and 3 mL of complete DMEM was added in each well to allow media exchange between the two compartments (overnight, 37°C, 5% CO_2). Cells were co-cultured up to 48 hours (37°C, 5% CO_2).

2.5.1 Nanoparticle kinetics of internalization in co-culture: flow cytometry. Cells were incubated with DY547-NP (125 μg/mL in complete cell culture media) corresponding to a final 40 nM siRNA concentration, up to 48 hours (37°C, 5% CO_2). After each time point (4, 12, 24 and 48 h), NP containing medium was removed, cells were washed with PBS (n=3) and detached using Trypsin-EDTA solution (#59417C, Sigma-Aldrich, UK) for 10 min at room temperature. Note that trypsin was used to remove any residual membrane-bound nanoparticle, enabling the detection of internalized DY547-NP only. Cells were pelleted (1000 rpm, 5 min, 25°C) and re-suspended in 400 μL PBS. The internalization of DY547-NP was determined on 10,000 individual and live cells with the BD LSRFortessa cytometer (BD Bioscience, San Jose CA, USA) equipped with the FACSDiva software (v8.0.1). Data were analyzed with FlowJo (vX.0.7, Tree Star, Ashland, OR, USA) after gating single and live events in the FSC-A/FSC-H and FSC/SSC windows, respectively. Untreated cells were used as autofluorescence control in order to calculate the median fluorescence intensity (MFI) fold

change over time, as well as the percentage of positive events for each cell line. Untreated cells were also used as a control.

2.6 Imaging: CD44, nanoparticle internalization and siRNA localization

2.6.1 CD44 expression: inverted microscope. Images of IF samples were acquired using an inverted microscope (Leica DMI6000B, Leica Microsystems, UK) coupled with a 5.5 Neo sCMOS camera (Andor, UK) and the EL6000 fluorescent lamp (Leica Microsystem, UK), all controlled by *μManager* software (v.1.46, Vale Lab, UCSF, USA). For acquisitions, immersion oil 63X/1.40-0.60 HC PL Apo objective was used, using I3 filter cube (Leica Microsystem, UK). Images were post-processed using ImageJ adjusting brightness/contrast for a better visualization of CD44 (v1.51h, http://imagej.nih.gov/ij).

2.6.2 Nanoparticle internalization: confocal microscope. An inverted SP5 laser scanning confocal microscope (Leica TSC SP5 AOBS, Leica Microsystem, UK) was used to acquire volumetric datasets of IF stained cells. Acquisitions were performed using the immersion oil 63X/1.40 HCX PL Apo objective. Images were acquired with sequential scan using 405, 488, 546 and 594 nm laser lines. Images were acquired with different settings accordingly to each experiment, in particular pinhole was kept to 1 airy unit aperture, pixel size adjusted to 150-165 nm, laser lines settings were adjusted to the dyes, frequency scan and averaged line were modified accordingly to the sample, whether live or fixed. Images were post-processed using ImageJ adjusting brightness/contrast for a better visualization of components (v1.51h, http://imagej.nih.gov/ij). Large field images were also used to quantify the amount of siRNA internalized: briefly, the maximum projection of the siRNA channel was obtained, Otsu threshold was applied, the area of the signal was measured and expressed as % with respect to the scanned area.

2.7 siRNA delivery and KRAS silencing

NP (0.125 mg/mL, final concentration in complete cell culture media) were used for KRAS silencing experiments. NP were prepared loading 40 nM (corresponding to 0.5 μg/mL) of L3-

siRNA sequence (sense 5'-3': GGACUCUGAAGAUGUACCU[dT][dT] 21nt, standard purification, Sigma-Aldrich, UK). Refer to the Supplementary Information for detailed description of siRNA sequences tested for KRAS silencing (Section SI.2). Briefly, HCT-116 cells were seeded at a density of 10,000 cells/cm^2 in TCP 12-well plates with flat bottom (Thermo Scientific, NUNC MULTIDISH 12, #150628) and left adhere overnight. Cells were then incubated in complete media containing NP (HA-coated) for 48 hours in a humidified 5% (v/v) CO_2 air atmosphere at 37°C. In the case of Nanocin NP, the media was changed after 24 hours, which has been found to improve the silencing efficiencies. Nanocin is compatible with repeat transfection due to relatively low cell toxicity. Lipofectamine™ 2000 was used as control. NP containing media were removed and cells thorough rinsed with PBS (n=3). The total RNA was extracted using phenol-chloroform method with: TRI Reagent (Cat. No.: T9424, Sigma-Aldrich). Reverse Transcription Reaction was performed using kit: High Capacity RNA-to-cDNA kit, Applied Biosystems and finally amplification (qPCR) was performed using kit: 2xqPCRBIO SyGreen Mix Lo-ROX (Cat.No. PB20.11-05, Applied Biosystems, UK) following manufacturer's instructions.

2.8 Statistical Analysis

Differences between groups were considered to be significant at a P value of <0.05. Statistical analyses (One-way ANOVA) were performed with GraphPad Prism 7.0 (GraphPad Software, Inc., San Diego, CA).

3. Results and Discussion

3.1 Nanoparticles characterization

3.1.1 Nanoparticle physical stability. As prepared, all NP showed a rather comparable hydrodynamic size, although typically lower for Nanocin (Table 1, Figure 1a and 1b). This is likely due to the higher charge density of this polymer, which allows a higher ionic cross-link density and therefore also a lower water content in the particles. As expected, the ζ-potential (surface charge) depended on the polycation:HA weight ratio, and shifted from positive to negative values with increasing HA content. With both polycations, a 'charge inversion' occurred at a polycation:HA weight ratio between 1:1 and 1:2; these samples also exhibited the largest sizes. At stoichiometry ratios close to the effective complexation between positive and negative charges, polyelectrolyte complexes form and keep aggregating due to the reduced repulsion, until a size is reached. At this equilibrium, a small imbalance in either of the charged components leads to a sufficient surface coverage to grant electrostatic stabilization. In deionized water, chitosan-based NP showed a mild agglomeration upon storage (size variation less than 5%), independent of the amount of HA. On the contrary, Nanocin stability depended on HA: Better stability at high HA content which decreased at low (polycation:HA < 1:2), and showed significant increases in size and ζ-potential post storage. This effect is probably due to the strong interactions between the high-cationic density, small-size Nanocin and HA, which significantly reduce the electrostatic stabilization due to excess (uncomplexed) negative charges of HA. Due to their better stability, all further experiments were conducted with a 1:4 polycation/HA ratio.

Table 1. Effect of storage in water on the size and charge of nanoparticles with variable polycation:HA weight ratio.

Polycation:HA [a] (weight ratio)		Size (nm) [b]		ζ-potential (mV) [b]	
		As prepared	Stored [c]	As prepared	Stored [c]
1:0	*chitosan*	210 ± 5	210 ± 5	52.0 ± 1.5	52.0 ± 1.0
	Nanocin	120 ± 10	390 ± 100	15.5 ± 7.5	24.0 ± 0.5
1:1	*chitosan*	270 ± 10	300 ± 15	35.0 ± 1.0	35.0 ± 1.0
	Nanocin	170 ± 10	400 ± 10	21.0 ± 1.0	23.0 ± 1.0
1:2	*chitosan*	220 ± 5	205 ± 5	-25.5 ± 0.5	-24.5 ± 1.0
	Nanocin	210 ± 75	320 ± 10	-19.0 ± 1.5	-21.0 ± 0.5

1:3	*chitosan*	230 ± 5	255 ± 15	-31.0 ± 1.0	-32.5 ± 1.0
	Nanocin	180 ± 20	185 ± 5	-30.0 ± 0.5	-31.5 ± 0.5
1:4	*chitosan*	275 ± 5	280 ± 5	-34.5 ± 0.5	-35.0 ± 1.0
	Nanocin	160 ± 10	170 ± 5	-30.0 ± 1.0	-30.5 ± 1.0

[a] Please note that siRNA was always used at a ratio 2.3%wt. in respect to the polycation weight, hence nanoparticles were prepared also in the absence of HA.
[b] Concentration: 1 mg/mL in deionized water
[c] Storage: 1 week, 4°C in deionized water.

342 *3.1.2 Protection of siRNA against RNase*. We have assessed the stability of siRNA in
343 nanoparticles (siRNA:polycation 1:4 weight ratio), when they were exposed to different
344 concentrations of RNase I (Figure 1e). siRNA in solution was already partially degraded at
345 0.01 U/μL RNase (~10% degradation), with >50% degradation at 0.1 U/μL RNase, whereas
346 siRNA liberated from nanoparticles was intact even after exposure to 1 U/μL RNase, with no
347 statistically relevant difference with the two polycations and with/out HA.
348

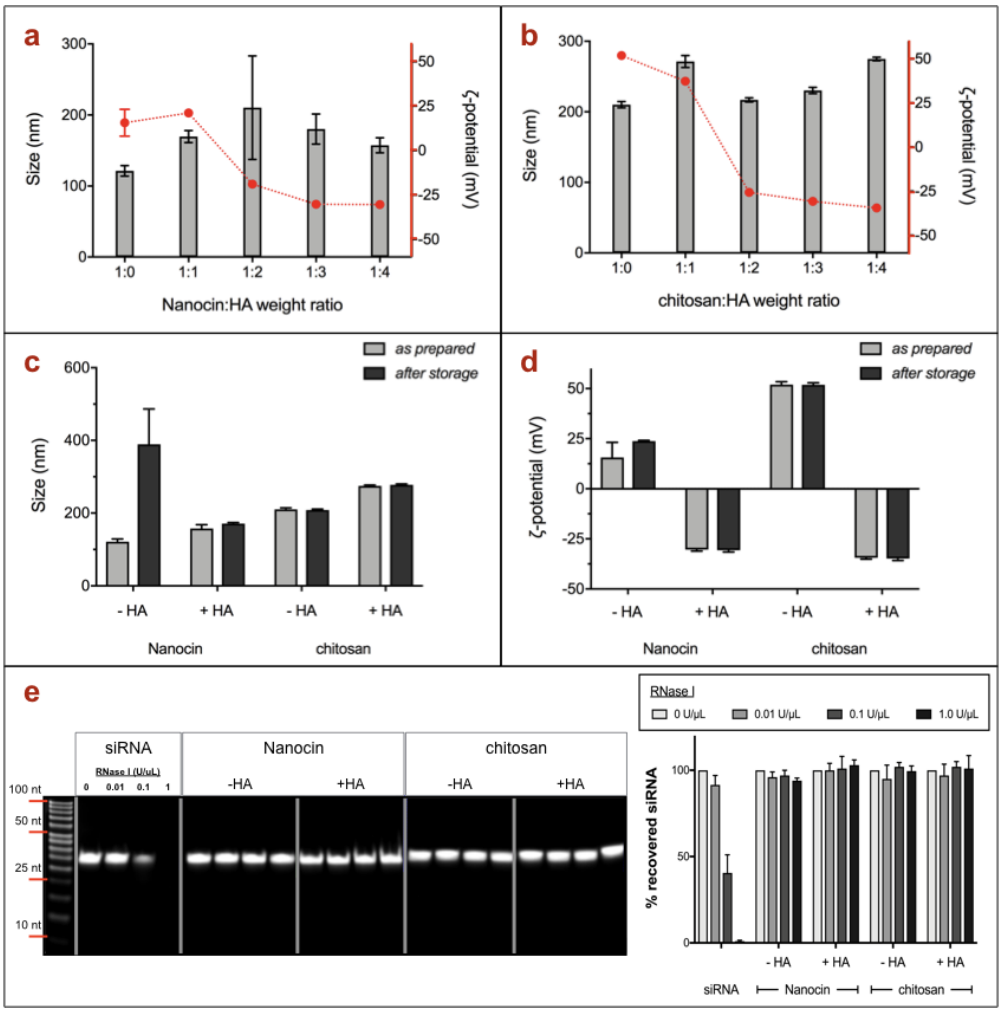

Figure 1. *Physico-chemical characterization of nanoparticles. Z-average size (histogram) and ζ-potential (red dots) of as-prepared Nanocin- (a) and chitosan-based (b) nanoparticles. The effect of storage is respectively shown in (c) and (d) for particles without HA and a 1:4 polycation:HA ratio. A typical PAGE gel analysis (e) shows payload protection for 25% wt. siRNA-loaded nanoparticles after incubation with different concentrations of RNase I (for each column, from left to right: 0, 0.01, 0.1, 1 U/µL). Recovered siRNA is expressed as percentage with respect to its control, each value is reported as average ± st.dev. of at least three independent samples.*

3.2 Targeting and internalization of HA-coated nanoparticles

3.2.1 CD44 expression. Colorectal cancers have a high incidence of mutation of KRAS, and we have therefore chosen a model of human colorectal cancer, HCT-116 cells, known to present $KRAS^{G13D}$ mutation (Alves et al., 2015). HCT-116 also have high CD44 expression (Rios de la Rosa et al., 2017b), and unsurprisingly this is higher than in the cells (HDFa) which we used as a model for stromal component of the tumor microenvironment (Figure 2a). Importantly, HCT-116 cells were positive to CD44 variants commonly associated to

malignancies, such as CD44v3^{high} (Figure 2c) and CD44v6 ^{high} (Figure 2e), but not CD44v4 (Figure 2d). No CD44 variants were detected in HDFa (data not shown).

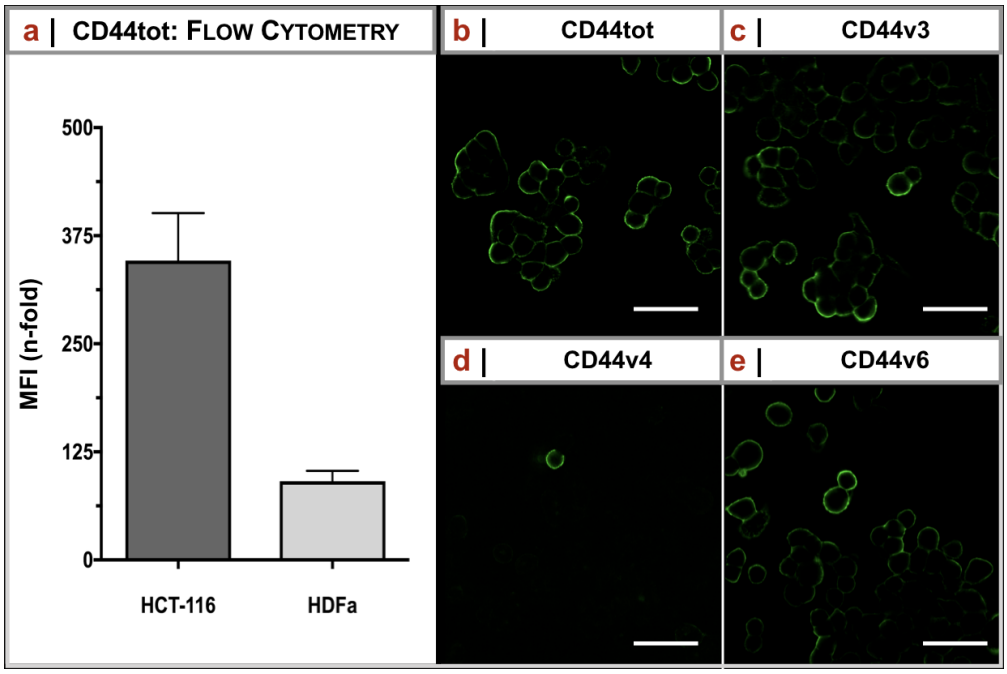

Figure 2. *Characterization of CD44 expression in the selected cellular models. a) Flow cytometry measurements of total CD44 (all isoforms combined) in HCT-116 and HDFa. Results are expressed as mean ± st.dev. (n=3, N=2). Immunofluorescence (IF) cancer cells (HCT-116) stained for: b) total CD44, c) CD44v3, c) CD44v4 and e) CD44v6. Scale bars 50 µm.*

3.2.2 Nanoparticle internalization: mono-culture vs. co-culture. We have followed the kinetics of both NP internalization via flow cytometry using a fluorescently labelled siRNA (L3-DY547-NP) for 24 h. NP internalization was firstly investigated on cancer cells and fibroblasts in mono-culture, then cells were co-cultured. In mono-culture of both cell types, chitosan/HA NP showed a more rapid internalization, however eventually reaching a plateau, as already seen in previous works (Lallana et al., 2017; Rios de la Rosa et al., 2017a). At the later time points the fluorescence intensities produced by the siRNA were comparable in both carriers (Figure 3). Qualitatively, in co-culture we observed a similar kinetic behavior, i.e. an earlier plateau for chitosan/HA. However, assuming that the siRNA fluorescence always provides quantitative and comparable estimates of NP internalization, we noticed another more interesting phenomenon: in mono-culture the uptake in HDFa and HCT-116 appeared to be comparable (Figure 3a) between the tested NP, whilst in co-culture HCT-116 always

internalized NP in much larger amounts (Figure 3b). Of note, where internalization in HCT-116 always increased in co-culture, the internalization in HDFa increased for Nanocin/HA and decreased for chitosan/HA, which means that although this HCT-116/HDFa differential internalization (and targeting) was clear for both NP, it was much larger with chitosan/HA systems. Mechanistically, this may be due an increased expression of CD44 and/or its variants: we have demonstrated that the overall CD44 expression depends on the HCT-116 environment (3D culture increasing it) (Rios De La Rosa et al., 2018), whereas interactions with cancer associated fibroblasts have been reported to increase CD44v expression in colon cancer cells (Misra et al., 2011). Therapeutically, this is a very promising result, which indicates that HA-coated formulations may be able to preferentially target and treat populations of tumoral cells, thereby effectively reducing potential off-target effects. Additionally, preliminary toxicology results showed no cytotoxicity (see Supplementary Information, section SI.10 and Figure 5SI) or increased levels of cellular stress (see Supplementary Information, section SI.11 and Figure 6SI). These results indicate that both nanoparticles are suitable for further *in vivo* studies.

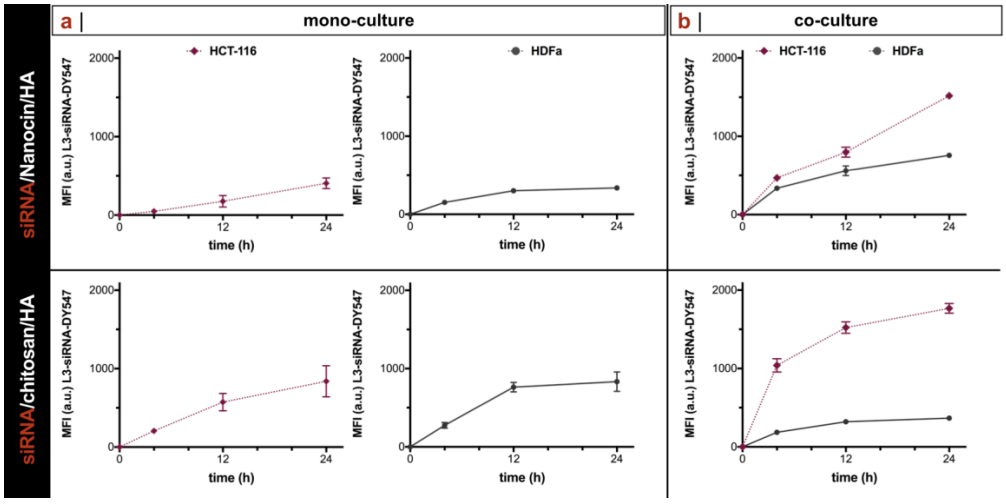

Figure 3. *Kinetics of internalization of HA-coated* L3-DY547-NP *in CD44-expressing cell lines: cancer (HCT-116, CD44^{+}, CD44v6^{high}) and fibroblasts (HDF, CD44^{low}). Results are expressed as mean ± st.dev. of 10,000 events (n=3 independent samples) at each time point. In mono-culture, similar kinetics of uptake are observed in both cell lines and for both NP. Whereas, a more tumor-like environment (co-culture of HCT-116 and HDFa) promotes a higher internalization of HA-coated NP, with increased uptake in cancer cells rather than fibroblasts at each time point (fold increase of 2-3 at the endpoint).*

385 *3.2.3 Intracellular localization*. At a very early time point (1 h), despite the different
386 internalization kinetics recorded through flow cytometry, chitosan/HA and Nanocin/HA NP
387 did not showed a markedly different behavior: both of them were internalized in similar
388 amounts with some, possibly initial signs of colocalization with lysosomal compartments
389 (Figure 4a). This snapshot evidenced initial NP localization in lysosomes (yellow from
390 contemporaneous emission of Lysotracker (green, 488nm) and siRNA (red, 561 nm), but also
391 signs of possible escape (red siRNA signal around or flanking the yellow or green
392 organelles). At 24 h, the two HA-decorated L3-DY547-NP are internalized/accumulated in
393 HCT-116 in similar amounts (Figure 4b; n=5 fields of view, average of 150 cells observed for
394 each treatment), which is broadly in line with the flow cytometry results. Of note, the siRNA
395 cytosolic distribution seemed to be consistently more homogeneous with chitosan/HA NP,
396 and more compartmented (visibly brighter spots) with Nanocin/HA NP. This phenomenon
397 may indicate a possibly lower availability of siRNA in the Nanocin/HA at this stage, which
398 would stem from a tighter complexation of the nucleic acid with the polycation. This tight
399 interaction would be possibly caused by: a) the higher charge density on Nanocin and b) its
400 lower size. The higher charge density of the polycation may cause a higher avidity; a more
401 compact siRNA/polycation complex is possibly obtained with Nanocin (smaller Mw) that has
402 an easier complexation compared to the larger polyelectrolytes (chitosan, entropic penalty for
403 surface siRNA/polycation coupling) However, we should also consider that any factor
404 increasing the complexation strength, such as a high charge density, is not necessarily
405 detrimental: for example, using chitosan we have recently demonstrated that high density of
406 amines increased chitosan binding to RNAs, but this effect was most likely overcome by
407 higher endosomolytic efficiency (Lallana et al., 2017).

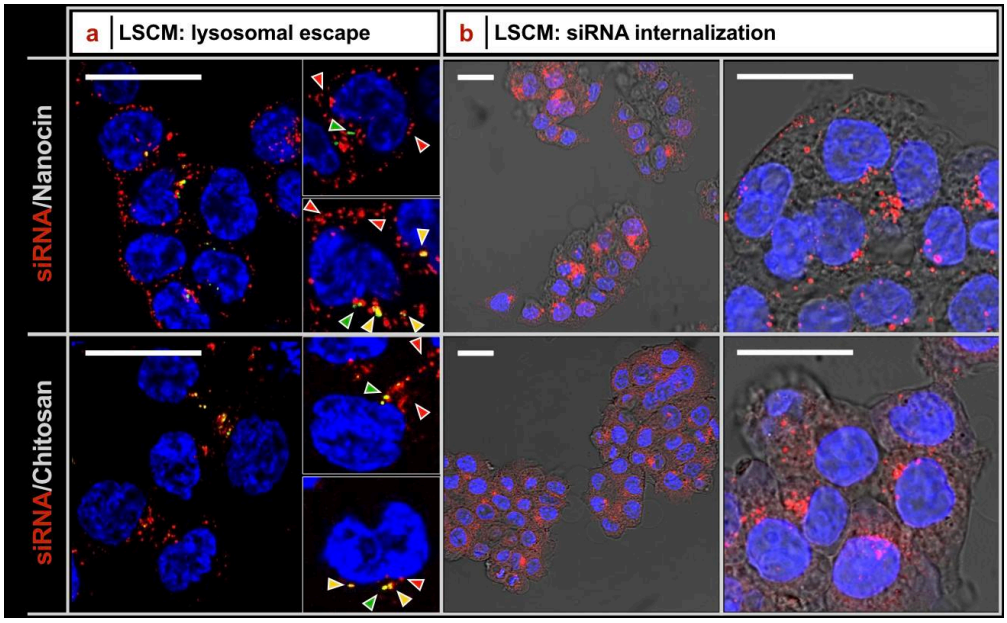

Figure 4. Nanoparticle and siRNA intracellular localization: a) lysosomal escape after 1 h incubation with NP, the arrows indicate lysosomes (green), the co-localization of nanoparticles in late endosomes/lysosomes (yellow) and released siRNA (red); b) internalization of siRNA in HCT-116 cells after 24 h incubation with NP, notably a similar percentage of siRNA was delivered in HCT-116, being 3.35% and 3.55% respectively for Nanocin/HA and chitosan/HA NP; a more 'cloudy' siRNA signal was observed in HCT-116 cells incubated with chitosan/HA NP, compared to a more localized siRNA signal for the Nanocin/HA counterparts. Scale bars: 25 µm.

3.3 Silencing efficacy: siRNA release from nanoparticles and mRNA-KRAS knock-down

3.3.1 Choice of siRNA. We have first investigated the silencing efficiency of a panel of different siRNA, employing simple Nanocin/siRNA polyplexes, since their high positive charge (see Table 1) was supposed to stimulate the highest transfection. The silencing efficiency was evaluated with qRT-PCR, rather than immunostaining methods, due to its superior sensitivity; this is critical in KRAS analysis as the level of gene expression is low and therefore difficult to detect. We eventually selected the GGACUCUGAAGAUGUACCUAGGUACAUCUUCAGAGUCCs sequence as a promising and more reproducible candidate for further experiments, after comparison of the silencing efficiencies of 14 siRNAs targeting different regions within the mRNA sequences (see Supplementary Information, section SI.2 and Figure 1SI).

3.3.2. KRAS-silencing. Chitosan/HA NP resulted in KRAS silencing to a level comparable to the gold standard transfecting agent Lipofectamine (no statistical difference between the two

treatments at 48 h, Figure 5a); more importantly, the mRNA-KRAS reduction was approximately 2-fold higher than with Nanocin/HA. As anticipated in section 3.2.3, the higher charge density of Nanocin may be a limiting factor for siRNA intracellular availability, which is a possible explanation for its lower silencing activity. Of interest, the HA-decorated NP caused levels of silencing similar to those of the binary polyplexes, i.e. siRNA/polycation only (see Supplementary Information, Figure 2SI); the latter are cationic species, and as such are characterized by an efficient cell adhesion and penetration, therefore it is remarkable that HA, most likely through its interactions with CD44, allows to overcome the effect of charge inversion.

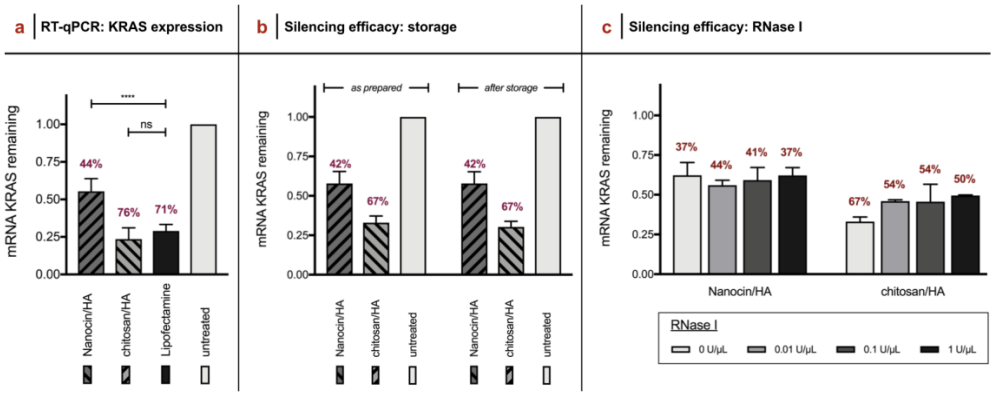

Figure 5. KRAS silencing efficacy of HA-coated NP. Relative KRAS expression and mRNA silencing was measured after 48 h treatment in HCT-116 cells with: a) *as prepared* NP: results show no statistical difference of chitosan-nanoparticles with respect to lipofectamine and a significant difference between Nanocin NP and lipofectamine (n=5, $p<0.0001$); b) NP after one-week storage at 4°C generally showed a silencing efficacy similar to that of *as prepared* NP. Data are expressed as percentage with respect to untreated cells and are the average on n=3 independent experiments. Lipofectamine was used as control (data not reported); c) NP exposed (incubation prior use) to RNase I at different concentrations (0, 0.01, 0.1, 1 U/µL). Data are expressed as percentage with respect to untreated cells and are the average on n=3 independent experiments. Lipofectamine was used as control (data not reported).

3.3.3 Effect of storage on silencing efficacy. NP were also stored for 1 week at 4°C in deionized water before using them in silencing experiments; this storage period caused no significant alteration in the silencing activity of both NP (Figure 5b). Interestingly, we observed that without HA (direct complexation between siRNA and polycations) the chitosan-based NP experienced a significant reduction in silencing performance (from >60% to about 40%, Supplementary Information Figure SI2), which is likely to ascribe to the low

437 degree of protonation of chitosan amines, which eventually allows self-aggregation of the
438 polymer and physical destabilization of the particles.
439
440 *3.3.3 Effect of RNase I exposure on silencing performance*. As a last step in the assessment of
441 NP for *in vivo* administration, we tested whether siRNA loaded in Nanocin- and chitosan-NP
442 could preserve its silencing functionality when the NP are exposed to potentially RNA-
443 degrading condition, such as the presence of RNAse. To support our previous demonstration
444 that the apparent integrity of the loaded siRNA (Figure 1e) ensures the preservation of its
445 silencing capacity, we further tested the silencing efficiency of both NP after exposure to
446 different concentration of RNase I (i.e. 0.01, 0.1, 1 U/μL) and compared the results to non-
447 exposed NP (incubated in nuclease free water, control). In these experiments, concentrations
448 of RNAse up to 1 U/μL did not alter the performance of Nanocin/HA NP, whereas that of
449 chitosan/HA NP was in part decreased. This can be ascribed to the higher complexation
450 strength of Nanocin (higher charge density, lower molecular weight), which makes more
451 difficult for an enzyme to reach its target in the bulk of a particle. Indeed, similar effects can
452 be seen also for the polycomplexes formed without HA (see Supplementary information,
453 Figure 3SI).

454 **Conclusions**

455 We compared two HA-based polyplex systems for the delivery of siRNA in $CD44^+$ cell lines
456 (HCT-116 and HDFa), for a perspective KRAS-targeted tumor therapy. Our main findings are
457 that: a) $CD44^{high}/CD44v^+$ cancer cells (HCT-116) are more active for the internalization of
458 HA-coated NP than stromal standard $CD44^+$ cells (HDFa), and that this difference amplifies
459 when cells are co-cultured. This is a very encouraging finding that supports the use of HA for
460 tumor targeting, with potential low off-target effects; b) the strength of the polyelectrolyte
461 complexation is an important parameter that carries a delicate balance of favorable and
462 detrimental effects. The stronger interactions between Nanocin and siRNA (and HA) appear
463 to negatively affect the silencing efficacy of such NP, possibly due to the lower availability of

464 the nucleic acid. On the other hand, they most likely provide a higher stability against
465 nucleases (and other harmful agents for the nucleic acid). Remarkably, we found that chitosan
466 NP presented the right compromise between polyplexes stability and avidity/efficiency of
467 siRNA release, which conferred them a high silencing efficacy comparable to the gold
468 standard transfecting agent (i.e. Lipofectamine). With this rational, further *in vivo* studies will
469 need to demonstrate whether the different complexation also affects the stability of the NP in
470 the blood stream, and whether the higher silencing capacity of chitosan-based systems can be
471 confirmed in real tumors.

472 **Acknowledgement**

473 The NorthWest Centre of Advanced Drug Delivery (NoWCADD) established at the
474 University of Manchester in collaboration with AstraZeneca. Dr Enrique Lallana and Dr Julio
475 Rios de La Rosa are gratefully acknowledged for both discussions and experimental help. The
476 Bioimaging Facility of the Faculty of Life Sciences (University of Manchester) is maintained
477 with grants from BBSRC, Wellcome Trust, and the University of Manchester Strategic Fund.
478 This work was funded by the Innovate UK project number 101710.

479

References

Almalik, A., Day, P.J., Tirelli, N., 2013a. HA-coated chitosan nanoparticles for CD44-mediated nucleic acid delivery. Macromol. Biosci. 13, 1671–1680. https://doi.org/10.1002/mabi.201300302

Almalik, A., Karimi, S., Ouasti, S., Donno, R., Wandrey, C., Day, P.J., Tirelli, N., 2013b. Hyaluronic acid (HA) presentation as a tool to modulate and control the receptor-mediated uptake of HA-coated nanoparticles. Biomaterials 34, 5369–5380. https://doi.org/10.1016/j.biomaterials.2013.03.065

Alves, S., Castro, L., Fernandes, M.S., Francisco, R., Castro, P., Priault, M., Chaves, S.R., Moyer, M.P., Oliveira, C., Seruca, R., Corte-Real, M., Sousa, M.J., Preto, A., 2015. Colorectal cancer-related mutant KRAS alleles function as positive regulators of autophagy. Oncotarget 6, 30787–30802. https://doi.org/10.18632/oncotarget.5021

Appels, N., Beijnen, J., Schellens, J., 2005. Development of Farnesyl Transferase Inhibitors: A Review. Oncologist 10, 565–578. https://doi.org/10.1634/theoncologist.10-8-565

Asati, V., Mahapatra, D.K., Bharti, S.K., 2017. K-Ras and its inhibitors towards personalized cancer treatment: Pharmacological and structural perspectives. Eur. J. Med. Chem. https://doi.org/10.1016/j.ejmech.2016.09.049

Auzenne, E., Ghosh, S.C., Khodadadian, M., Rivera, B., Farquhar, D., Price, R.E., Ravoori, M., Kundra, V., Freedman, R.S., Klostergaard, J., 2007. Hyaluronic Acid- Paclitaxel: Antitumor Efficacy against CD44(+) Human Ovarian Carcinoma Xenografts. Neoplasia 9, 479–486. https://doi.org/10.1593/NEO.07229

Bassi, P.F., Volpe, A., D'Agostino, D., Palermo, G., Renier, D., Franchini, S., Rosato, A., Racioppi, M., 2011. Paclitaxel-hyaluronic acid for intravesical therapy of bacillus calmette-gurin refractory carcinoma in situ of the bladder: Results of a phase i study. J. Urol. 185, 445–449. https://doi.org/10.1016/j.juro.2010.09.073

Birzele, F., Voss, E., Nopora, A., Honold, K., Heil, F., Lohmann, S., Verheul, H., Le Tourneau, C., Delord, J.P., Van Herpen, C., Mahalingam, D., Coveler, A.L., Meresse,

507 V., Weigand, S., Runza, V., Cannarile, M., 2015. CD44 Isoform status predicts response
508 to treatment with Anti-CD44 antibody in cancer patients. Clin. Cancer Res. 21, 2753–
509 2762. https://doi.org/10.1158/1078-0432.CCR-14-2141
510 Blasco, R.B., Francoz, S., Santamaría, D., Cañamero, M., Dubus, P., Charron, J., Baccarini,
511 M., Barbacid, M., 2011. C-Raf, but Not B-Raf, Is Essential for Development of K-Ras
512 Oncogene-Driven Non-Small Cell Lung Carcinoma. Cancer Cell 19, 652–663.
513 https://doi.org/10.1016/j.ccr.2011.04.002
514 Chin, L., Tam, A., Pomerantz, J., Wong, M., Holash, J., Bardeesy, N., Shen, Q., O'Hagan, R.,
515 Pantginis, J., Zhou, H., Horner, J.W., Cordon-Cardo, C., Yancopoulos, G.D., DePinho,
516 R.A., 1999. Essential role for oncogenic ras in tumour maintenance. Nature 400, 468–
517 472. https://doi.org/10.1038/22788
518 Chindera, K., Mahato, M., Kumar Sharma, A., Horsley, H., Kloc-Muniak, K.,
519 Kamaruzzaman, N.F., Kumar, S., McFarlane, A., Stach, J., Bentin, T., Good, L., 2016.
520 The antimicrobial polymer PHMB enters cells and selectively condenses bacterial
521 chromosomes. Sci. Rep. 6, 23121. https://doi.org/10.1038/srep23121
522 Collins, M.A., Bednar, F., Zhang, Y., Brisset, J.-C., Galbán, S., Galbán, C.J., Rakshit, S.,
523 Flannagan, K.S., Adsay, N.V., Pasca di Magliano, M., Pasca, M., 2012. Oncogenic Kras
524 is required for both the initiation and maintenance of pancreatic cancer in mice. J. Clin.
525 Invest. 122, 639–653. https://doi.org/10.1172/JCI59227DS1
526 Collisson, E.A., Trejo, C.L., Silva, J.M., Gu, S., Korkola, J.E., Heiser, L.M., Charles, R.P.,
527 Rabinovich, B.A., Hann, B., Dankort, D., Spellman, P.T., Phillips, W.A., Gray, J.W.,
528 McMahon, M., 2012. A Central role for RAF→MEK→ERK signaling in the genesis of
529 pancreatic ductal adenocarcinoma. Cancer Discov. 2, 685–693.
530 https://doi.org/10.1158/2159-8290.CD-11-0347
531 Coradini, D., Pellizzaro, C., Miglierini, G., Daidone, M.G., Perbellini, A., 1999. Hyaluronic
532 acid as drug delivery for sodium butyrate: Improvement of the anti-proliferative activity
533 on a breast-cancer cell line. Int. J. Cancer 81, 411–416.
534 https://doi.org/10.1002/(SICI)1097-0215(19990505)81:3<411::AID-IJC15>3.0.CO;2-F

535 Cox, A.D., Fesik, S.W., Kimmelman, A.C., Luo, J., Der, C.J., 2014. Drugging the
536 undruggable RAS: Mission Possible? Nat. Rev. Drug Discov.
537 https://doi.org/10.1038/nrd4389
538 Culty, M., Nguyen, H.A., Underhill, C.B., 1992. The hyaluronan receptor (CD44) participates
539 in the uptake and degradation of hyaluronan. J. Cell Biol. 116, 1055–1062.
540 https://doi.org/10.1083/jcb.116.4.1055
541 Deng, X., Cao, M., Zhang, J., Hu, K., Yin, Z., Zhou, Z., Xiao, X., Yang, Y., Sheng, W., Wu,
542 Y., Zeng, Y., 2014. Hyaluronic acid-chitosan nanoparticles for co-delivery of MiR-34a
543 and doxorubicin in therapy against triple negative breast cancer. Biomaterials 35, 4333–
544 4344. https://doi.org/10.1016/J.BIOMATERIALS.2014.02.006
545 Ellis, C.A., Clark, G., 2000. The importance of being K-Ras. Cell. Signal.
546 https://doi.org/10.1016/S0898-6568(00)00084-X
547 Ganesh, S., Iyer, A.K., Morrissey, D. V., Amiji, M.M., 2013. Hyaluronic acid based self-
548 assembling nanosystems for CD44 target mediated siRNA delivery to solid tumors.
549 Biomaterials 34, 3489–3502. https://doi.org/10.1016/j.biomaterials.2013.01.077
550 Hatzivassiliou, G., Haling, J.R., Chen, H., Song, K., Price, S., Heald, R., Hewitt, J.F.M., Zak,
551 M., Peck, A., Orr, C., Merchant, M., Hoeflich, K.P., Chan, J., Luoh, S.M., Anderson,
552 D.J., Ludlam, M.J.C., Wiesmann, C., Ultsch, M., Friedman, L.S., Malek, S., Belvin, M.,
553 2013. Mechanism of MEK inhibition determines efficacy in mutant KRAS- versus
554 BRAF-driven cancers. Nature 501, 232–236. https://doi.org/10.1038/nature12441
555 Janes, K.A., Fresneau, M.P., Marazuela, A., Fabra, A., Alonso, M.J., 2001. Chitosan
556 nanoparticles as delivery systems for doxorubicin. J. Control. Release 73, 255–267.
557 https://doi.org/10.1016/S0168-3659(01)00294-2
558 Kamerkar, S., Lebleu, V.S., Sugimoto, H., Yang, S., Ruivo, C.F., Melo, S.A., Lee, J.J.,
559 Kalluri, R., 2017. Exosomes facilitate therapeutic targeting of oncogenic KRAS in
560 pancreatic cancer. Nature 546, 498–503. https://doi.org/10.1038/nature22341
561 Karousou, E., Misra, S., Ghatak, S., Dobra, K., Götte, M., Vigetti, D., Passi, A., Karamanos,
562 N.K., Skandalis, S.S., 2017. Roles and targeting of the HAS/hyaluronan/CD44

563 molecular system in cancer. Matrix Biol. https://doi.org/10.1016/j.matbio.2016.10.001
564 Kim, H., Yang, X.L., Rosada, C., Hamilton, S.R., August, J.T., 1994. CD44 expression in
565 colorectal adenomas is an early event occurring prior to K-ras and p53 gene mutation.
566 Arch. Biochem. Biophys. https://doi.org/10.1006/abbi.1994.1199
567 Lallana, E., Rios de la Rosa, J.M., Tirella, A., Pelliccia, M., Gennari, A., Stratford, I.J., Puri,
568 S., Ashford, M., Tirelli, N., 2017. Chitosan/Hyaluronic Acid Nanoparticles: Rational
569 Design Revisited for RNA Delivery. Mol. Pharm. 14, 2422–2436.
570 https://doi.org/10.1021/acs.molpharmaceut.7b00320
571 Li, F., Park, S.-J., Ling, D., Park, W., Han, J.Y., Na, K., Char, K., 2013. Hyaluronic acid-
572 conjugated graphene oxide/photosensitizer nanohybrids for cancer targeted
573 photodynamic therapy. J. Mater. Chem. B 1, 1678. https://doi.org/10.1039/c3tb00506b
574 Luo, Y., Bernshaw, N.J., Lu, Z., Kopecek, J., Prestwich, G.D., 2002. Targeted Delivery of
575 Doxorubicin by HPMA Copolymer-Hyaluronan Bioconjugates. Pharm. Res. 19, 396–
576 402. https://doi.org/10.1023/A:1015170907274
577 Ma, M., Chen, H., Chen, Y., Zhang, K., Wang, X., Cui, X., Shi, J., 2012. Hyaluronic acid-
578 conjugated mesoporous silica nanoparticles: excellent colloidal dispersity in
579 physiological fluids and targeting efficacy. J. Mater. Chem. 22, 5615.
580 https://doi.org/10.1039/c2jm15489g
581 Mao, S., Shuai, X., Unger, F., Simon, M., Bi, D., Kissel, T., 2004. The depolymerization of
582 chitosan: Effects on physicochemical and biological properties. Int. J. Pharm. 281, 45–
583 54. https://doi.org/10.1016/j.ijpharm.2004.05.019
584 Mattheolabakis, G., Milane, L., Singh, A., Amiji, M.M., 2015. Hyaluronic acid targeting of
585 CD44 for cancer therapy: From receptor biology to nanomedicine. J. Drug Target. 23,
586 605–618. https://doi.org/10.3109/1061186X.2015.1052072
587 Misra, S., Hascall, V.C., Berger, F.G., Markwald, R.R., Ghatak, S., 2008. Hyaluronan, CD44,
588 and cyclooxygenase-2 in colon cancer. Connect. Tissue Res.
589 https://doi.org/10.1080/03008200802143356
590 Misra, S., Heldin, P., Hascall, V.C., Karamanos, N.K., Skandalis, S.S., Markwald, R.R.,

591 Ghatak, S., 2011. Hyaluronan-CD44 interactions as potential targets for cancer therapy.
592 FEBS J. 278, 1429–1443. https://doi.org/10.1111/j.1742-4658.2011.08071.x
593 Parajó, Y., d'Angelo, I., Welle, A., Garcia-Fuentes, M., Alonso, M.J., 2010. Hyaluronic
594 acid/Chitosan nanoparticles as delivery vehicles for VEGF and PDGF-BB. Drug Deliv.
595 17, 596–604. https://doi.org/10.3109/10717544.2010.509357
596 Ponta, H., Sherman, L., Herrlich, P.A., 2003. CD44: From adhesion molecules to signalling
597 regulators. Nat. Rev. Mol. Cell Biol. 4, 33–45. https://doi.org/10.1038/nrm1004
598 Rios de la Rosa, J.M., Tirella, A., Gennari, A., Stratford, I.J., Tirelli, N., 2017a. The CD44-
599 Mediated Uptake of Hyaluronic Acid-Based Carriers in Macrophages. Adv. Healthc.
600 Mater. 6. https://doi.org/10.1002/adhm.201601012
601 Rios de la Rosa, J.M., Tirella, A., Gennari, A., Stratford, I.J., Tirelli, N., 2017b. The CD44-
602 Mediated Uptake of Hyaluronic Acid-Based Carriers in Macrophages. Adv. Healthc.
603 Mater. 6, 1601012. https://doi.org/10.1002/adhm.201601012
604 Rios de la Rosa, J.M., Tirella, A., Tirelli, N., 2018. Receptor-Targeted Drug Delivery and the
605 (Many) Problems We Know of: The Case of CD44 and Hyaluronic Acid. Adv. Biosyst.
606 2, 1800049. https://doi.org/10.1002/adbi.201800049
607 Rios De La Rosa, J.M., Wubetu, J., Tirelli, N., Tirella, A., 2018. Colorectal tumor 3D in vitro
608 models: advantages of biofabrication for the recapitulation of early stages of tumour
609 development. Biomed. Phys. Eng. Express 17.
610 Ross, S.J., Revenko, A.S., Hanson, L.L., Ellston, R., Staniszewska, A., Whalley, N., Pandey,
611 S.K., Revill, M., Rooney, C., Buckett, L.K., Klein, S.K., Hudson, K., Monia, B.P.,
612 Zinda, M., Blakey, D.C., Lyne, P.D., Macleod, A.R., 2017. Targeting KRAS-dependent
613 tumors with AZD4785, a high-affinity therapeutic antisense oligonucleotide inhibitor of
614 KRAS. Sci. Transl. Med. 9, eaal5253. https://doi.org/10.1126/scitranslmed.aal5253
615 Shin, W., Lee, S.K., Hwang, J.H., Park, J.C., Cho, Y.H., Ro, E.J., Song, Y., Seo, H.R., Choi,
616 K.Y., 2018. Identification of Ras-degrading small molecules that inhibit the
617 transformation of colorectal cancer cells independent of β-catenin signaling. Exp. Mol.
618 Med. 50, 71. https://doi.org/10.1038/s12276-018-0102-5

Stephen, A.G., Esposito, D., Bagni, R.G., McCormick, F., 2014. Dragging ras back in the ring. Cancer Cell. https://doi.org/10.1016/j.ccr.2014.02.017

Stylianopoulos, T., Jain, R.K., 2015. Design considerations for nanotherapeutics in oncology. Nanomedicine Nanotechnology, Biol. Med. https://doi.org/10.1016/j.nano.2015.07.015

Surace, C., Arpicco, S., Dufaÿ-Wojcicki, A., Marsaud, V., Bouclier, C., Clay, D., Cattel, L., Renoir, J.-M., Fattal, E., 2009. Lipoplexes Targeting the CD44 Hyaluronic Acid Receptor for Efficient Transfection of Breast Cancer Cells. Mol. Pharm. 6, 1062–1073. https://doi.org/10.1021/mp800215d

Überall, I., Kolář, Z., Trojanec, R., Berkovcová, J., Hajdúch, M., 2008. The status and role of ErbB receptors in human cancer. Exp. Mol. Pathol. https://doi.org/10.1016/j.yexmp.2007.12.002

Wang, Y., Kaiser, C.E., Frett, B., Li, H.Y., 2013. Targeting mutant KRAS for anticancer therapeutics: A review of novel small molecule modulators. J. Med. Chem. 56, 5219–5230. https://doi.org/10.1021/jm3017706

Yi Luo, †, Michael R. Ziebell, †,‡ and, Glenn D. Prestwich*, †, 2000. A Hyaluronic Acid−Taxol Antitumor Bioconjugate Targeted to Cancer Cells. https://doi.org/10.1021/BM000283N

Yu, M., Jambhrunkar, S., Thorn, P., Chen, J., Gu, W., Yu, C., 2013. Hyaluronic acid modified mesoporous silica nanoparticles for targeted drug delivery to CD44-overexpressing cancer cells. Nanoscale 5, 178–83. https://doi.org/10.1039/c2nr32145a

Zhang, Z., Jiang, G., Yang, F., Wang, J., 2006. Knockdown of mutant K-ras expression by adenovirus-mediated siRNA inhibits the in vitro and in vivo growth of lung cancer cells. Cancer Biol. Ther. 5, 1481–1486. https://doi.org/10.4161/cbt.5.11.3297

Zhao, P., Damerow, M.S., Stern, P., Liu, A.H., Sweet-Cordero, A., Siziopikou, K., Neilson, J.R., Sharp, P.A., Cheng, C., 2013. CD44 promotes Kras-dependent lung adenocarcinoma. Oncogene 32, 5186–5190. https://doi.org/10.1038/onc.2012.542

Zorde Khvalevsky, E., Gabai, R., Rachmut, I.H., Horwitz, E., Brunschwig, Z., Orbach, A., Shemi, A., Golan, T., Domb, A.J., Yavin, E., Giladi, H., Rivkin, L., Simerzin, A.,

Eliakim, R., Khalaileh, A., Hubert, A., Lahav, M., Kopelman, Y., Goldin, E., Dancour, A., Hants, Y., Arbel-Alon, S., Abramovitch, R., Shemi, A., Galun, E., 2013. Mutant KRAS is a druggable target for pancreatic cancer. Proc. Natl. Acad. Sci. 110, 20723–20728. https://doi.org/10.1073/pnas.1314307110

Supplementary Information

Click here to download Supplementary Material: SI-rev 01 2019 v2.docx

Figure 1

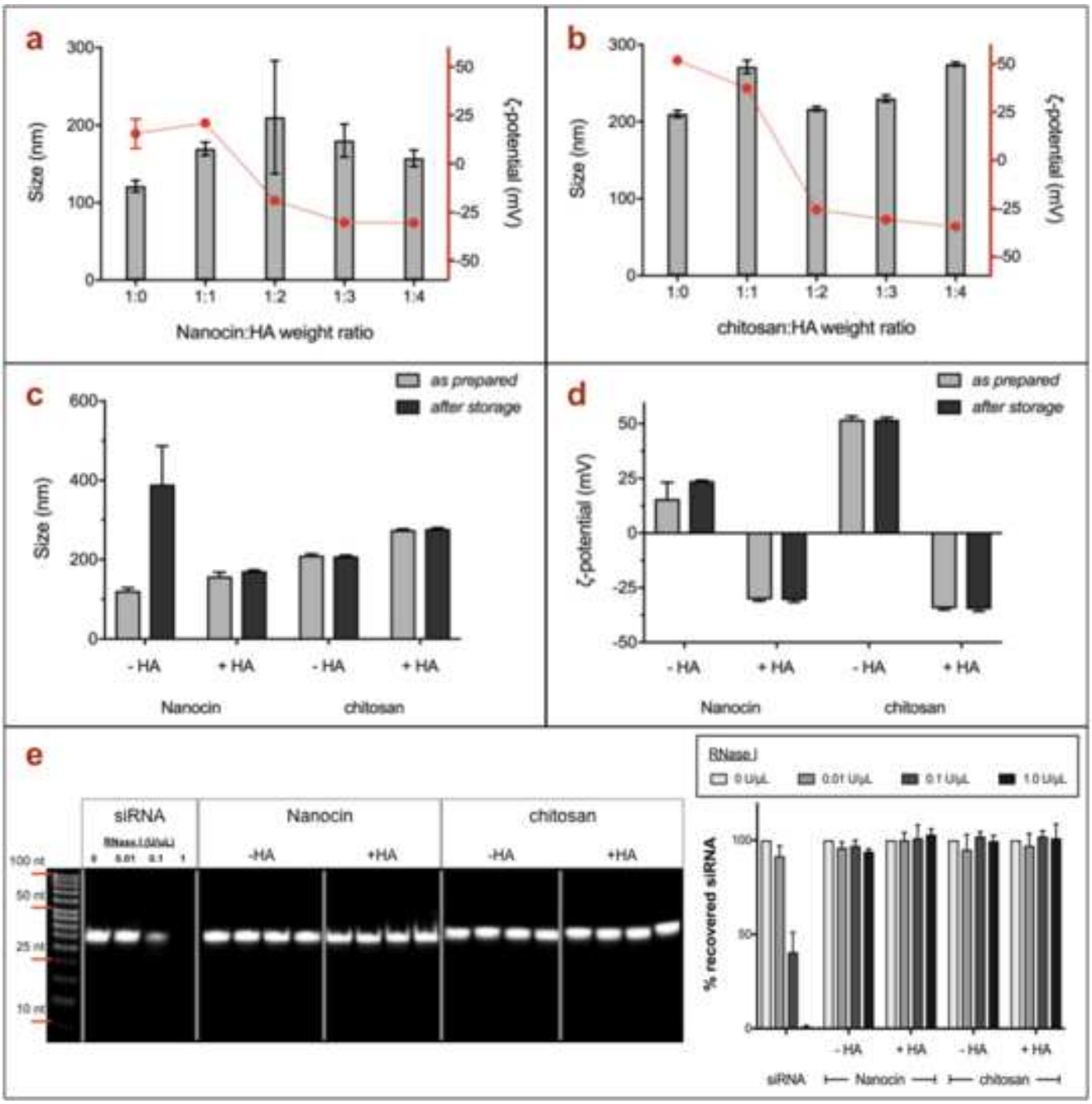
a
Size (nm)
ζ-potential (mV)
Nanocin:HA weight ratio
1:0
1:1
1:2
1:3
1:4
b
chitosan:HA weight ratio
c
as prepared
after storage
- HA
+ HA
Nanocin
chitosan
d
e
siRNA
Nanocin
chitosan
-HA
+HA
RNase.I
0 U/μL
0.01 U/μL
0.1 U/μL
1.0 U/μL
% recovered siRNA

Figure 2

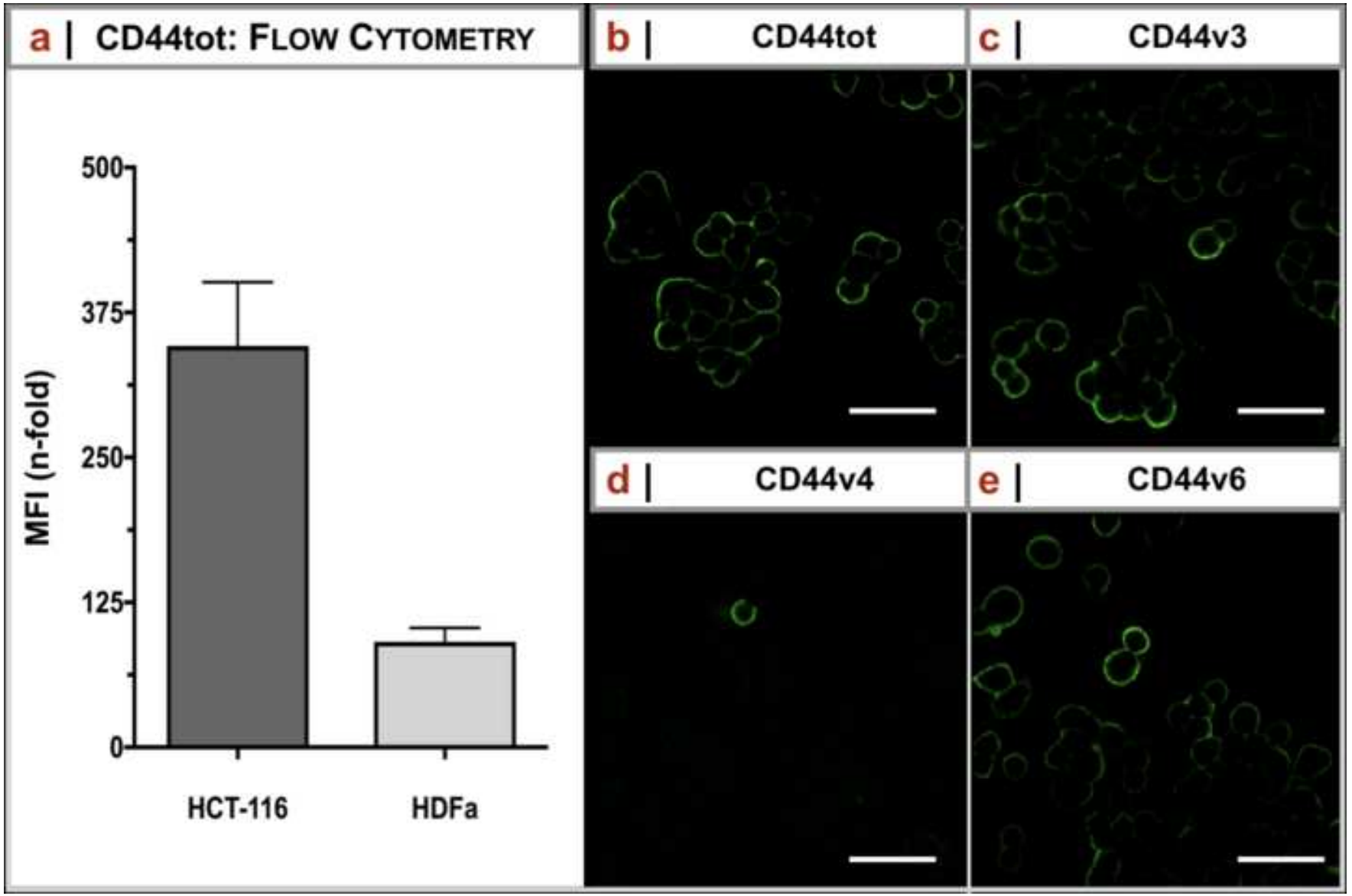
a | CD44tot: FLOW CYTOMETRY
MFI (n-fold)
500
375
250
125
0
HCT-116
HDFa
b | CD44tot
c | CD44v3
d | CD44v4
e | CD44v6

Figure 3

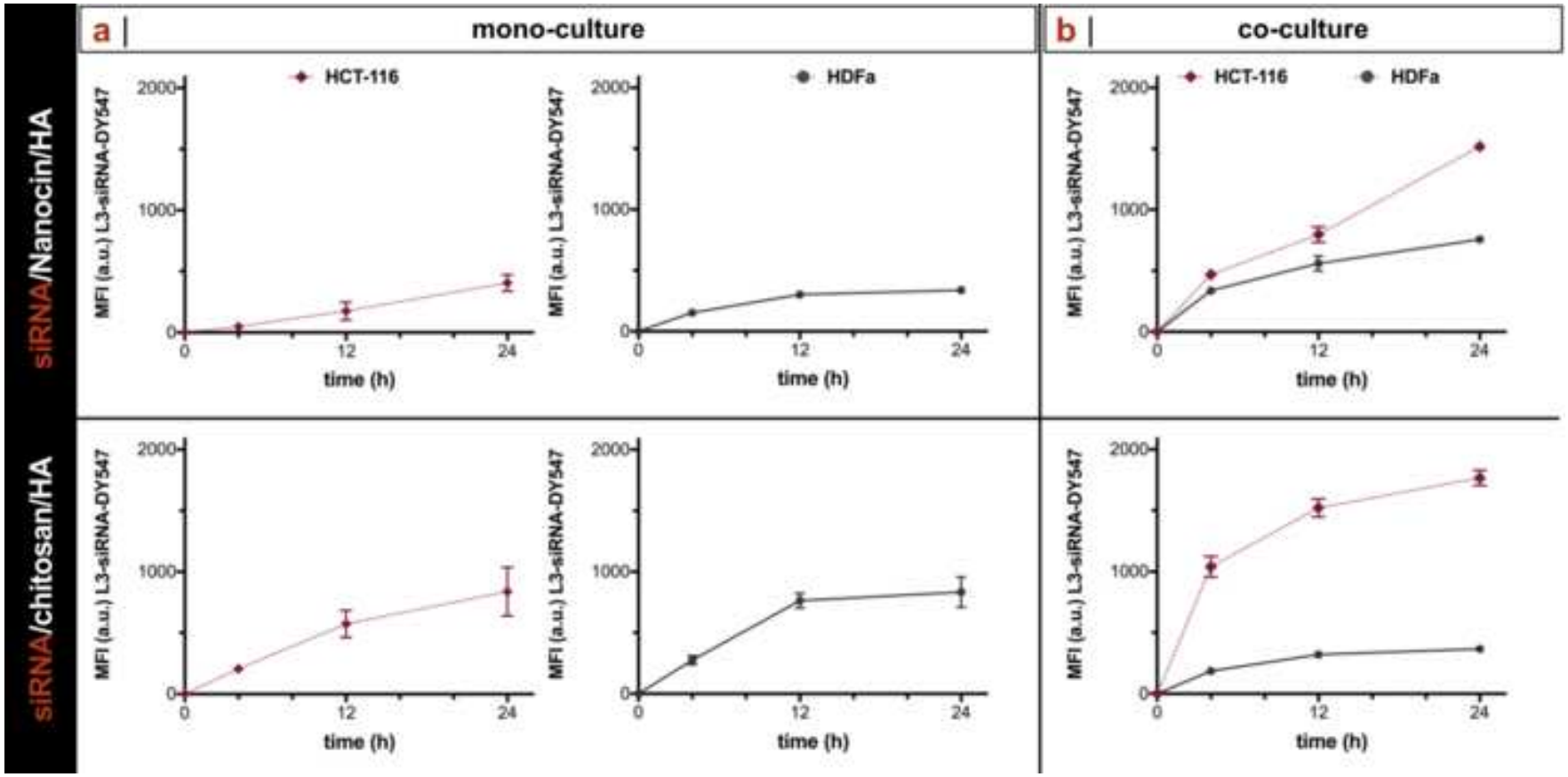
a |
mono-culture
b |
co-culture
siRNA/Nanocin/HA
siRNA/chitosan/HA
HCT-116
HDFa
MFI (a.u.) L3-siRNA-DY547
time (h)
0
1000
2000
12
24

Figure 4

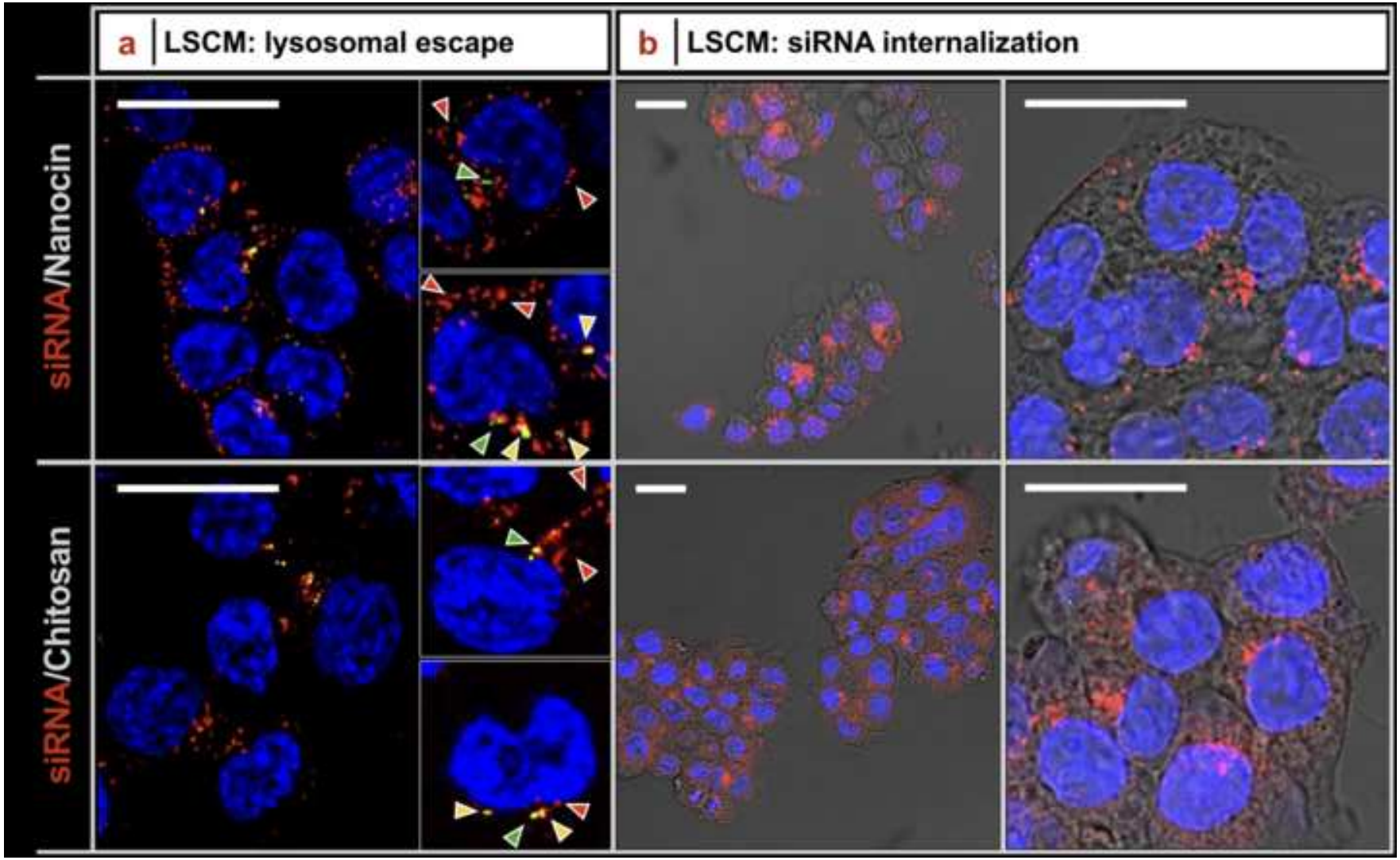
a
LSCM: lysosomal escape
b
LSCM: siRNA internalization
siRNA/Nanocin
siRNA/Chitosan

Figure 5

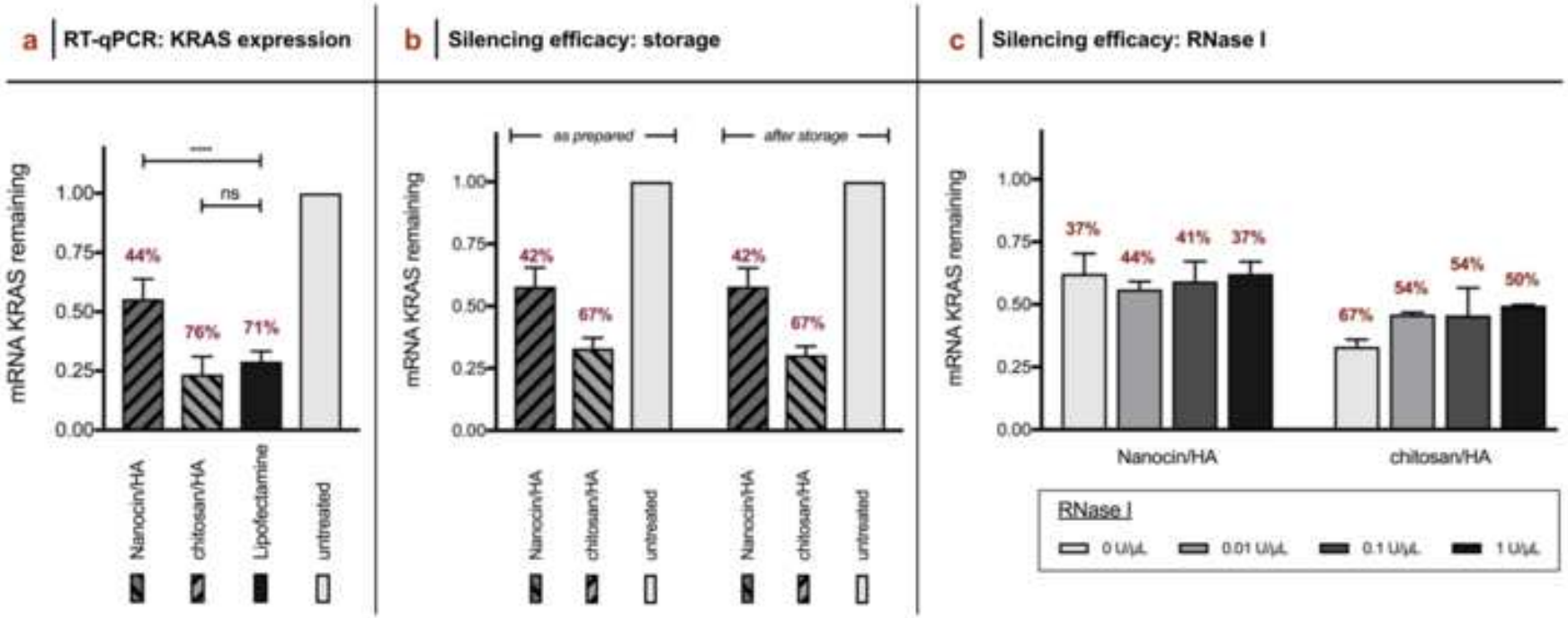
a | RT-qPCR: KRAS expression
mRNA KRAS remaining
1.00
0.75
0.50
0.25
0.00
****
ns
44%
76%
71%
Nanocin/HA
chitosan/HA
Lipofectamine
untreated
b | Silencing efficacy: storage
as prepared
after storage
42%
67%
42%
67%
c | Silencing efficacy: RNase I
37%
44%
41%
37%
67%
54%
54%
50%
Nanocin/HA
chitosan/HA
RNase I
0 U/µL
0.01 U/µL
0.1 U/µL
1 U/µL

Figure SI1

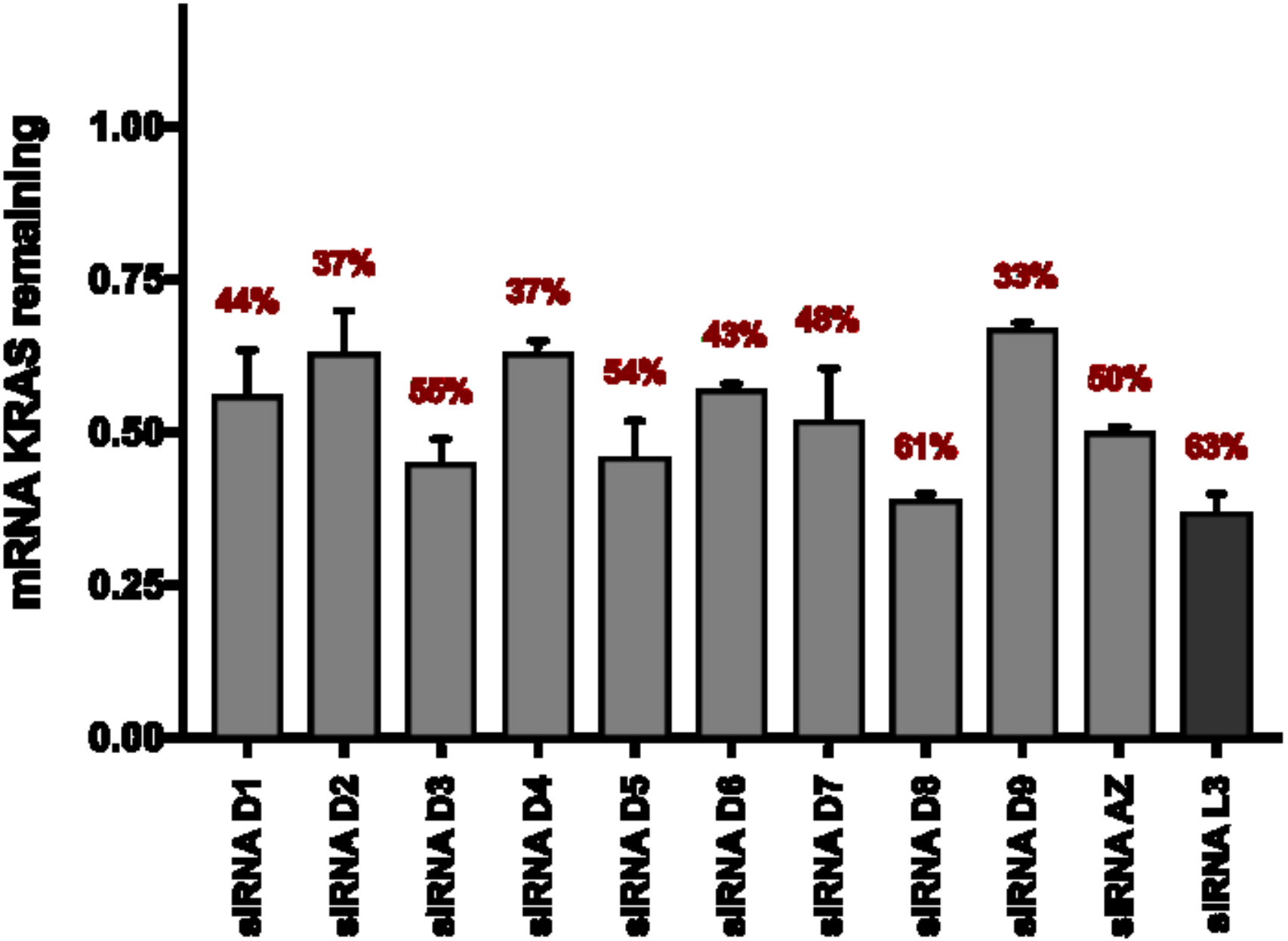
mRNA KRAS remalnlng
1.00
0.75
0.50
0.25
0.00
44%
37%
55%
37%
54%
43%
48%
61%
33%
50%
63%
siRNA D1
siRNA D2
siRNA D3
siRNA D4
siRNA D5
siRNA D6
siRNA D7
siRNA D8
siRNA D9
siRNA AZ
siRNA L3

Figure SI2

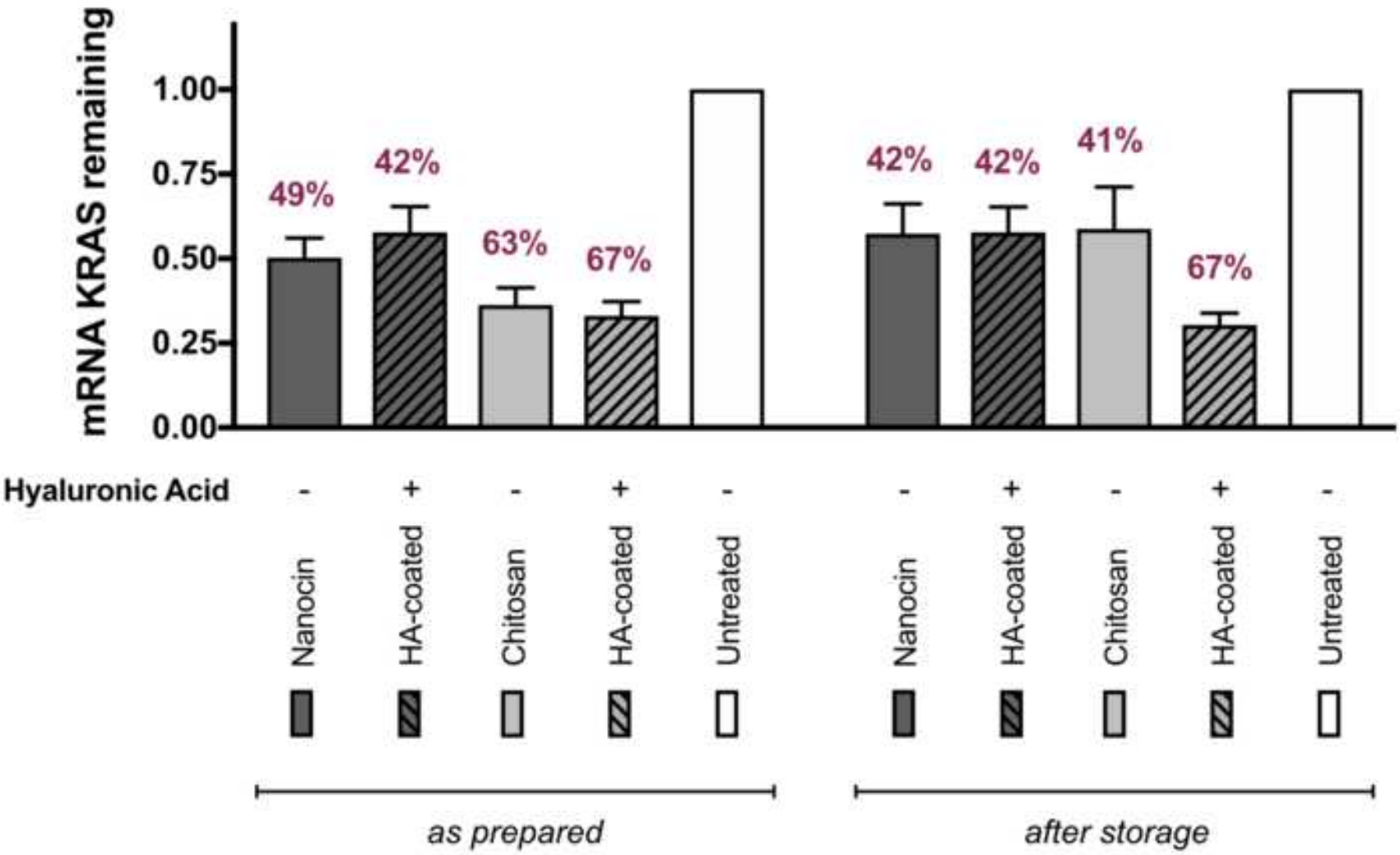
mRNA KRAS remaining
1.00
0.75
0.50
0.25
0.00
49%
42%
63%
67%
42%
42%
41%
67%
Hyaluronic Acid
-
+
-
+
-
-
+
-
+
-
Nanocin
HA-coated
Chitosan
HA-coated
Untreated
Nanocin
HA-coated
Chitosan
HA-coated
Untreated
as prepared
after storage

Figure SI3

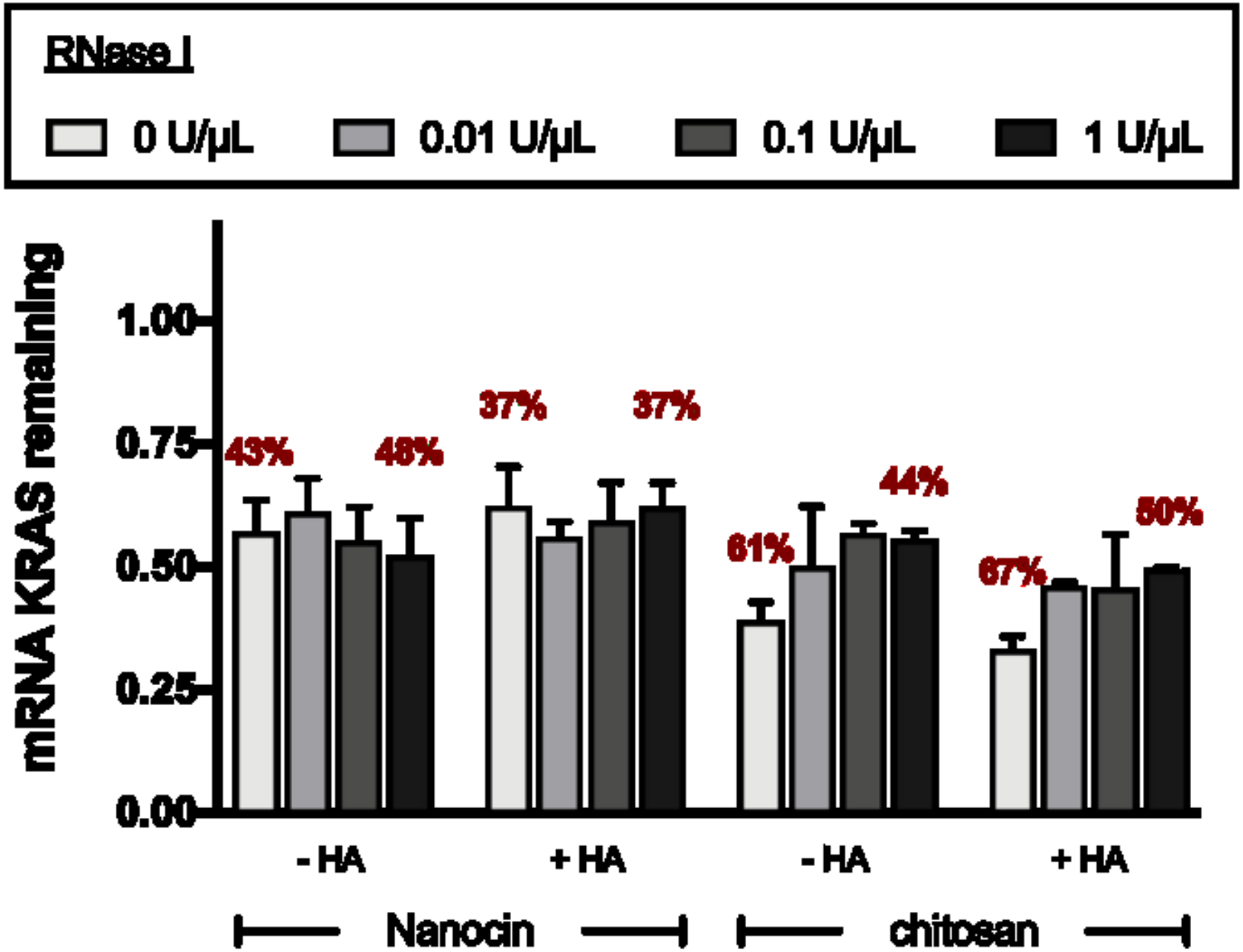
RNase I
0 U/µL
0.01 U/µL
0.1 U/µL
1 U/µL
mRNA KRAS remaining
1.00
0.75
0.50
0.25
0.00
43%
48%
37%
37%
61%
44%
67%
50%
- HA
+ HA
- HA
+ HA
Nanocin
chitosan

Figure SI4

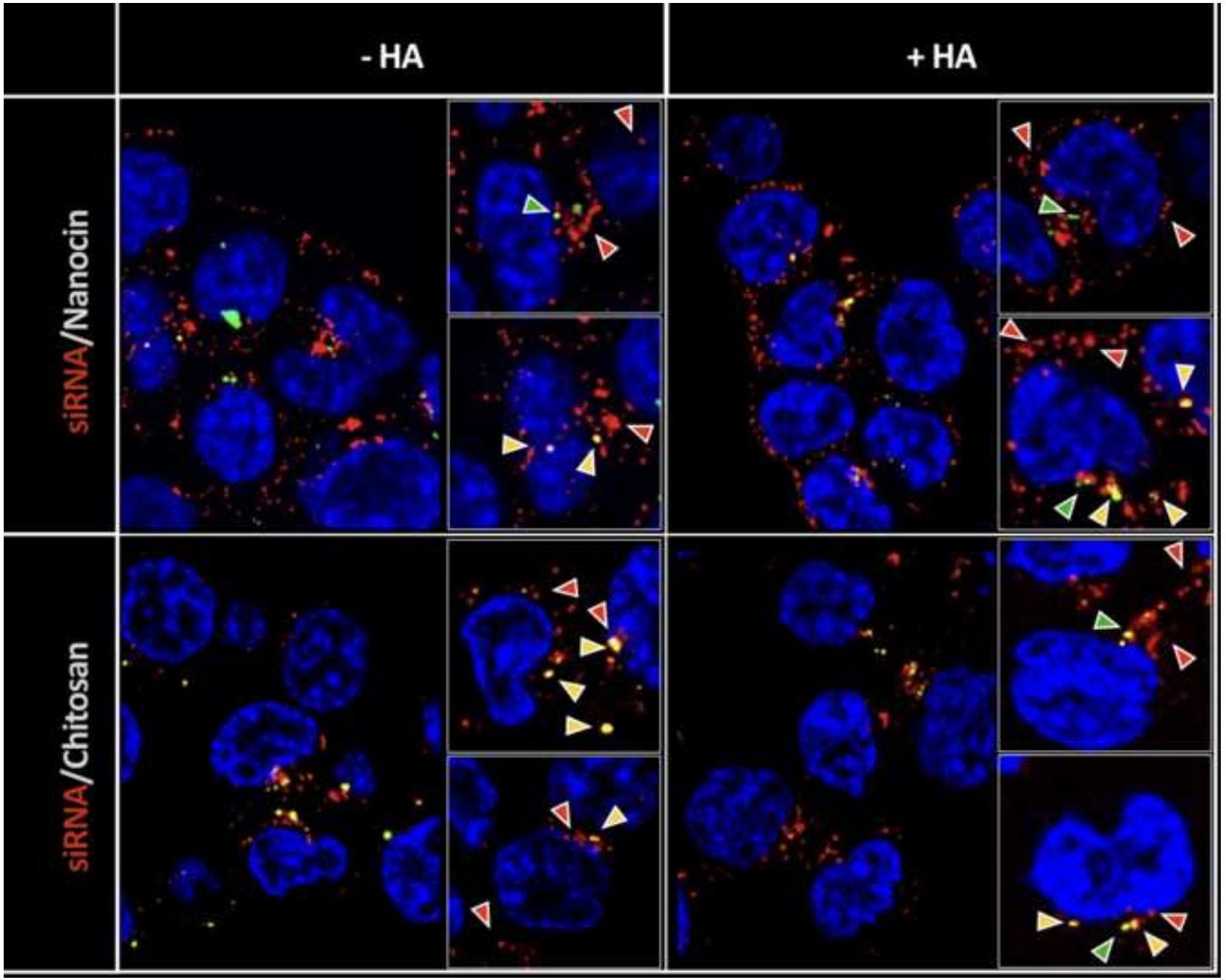

Figure SI5

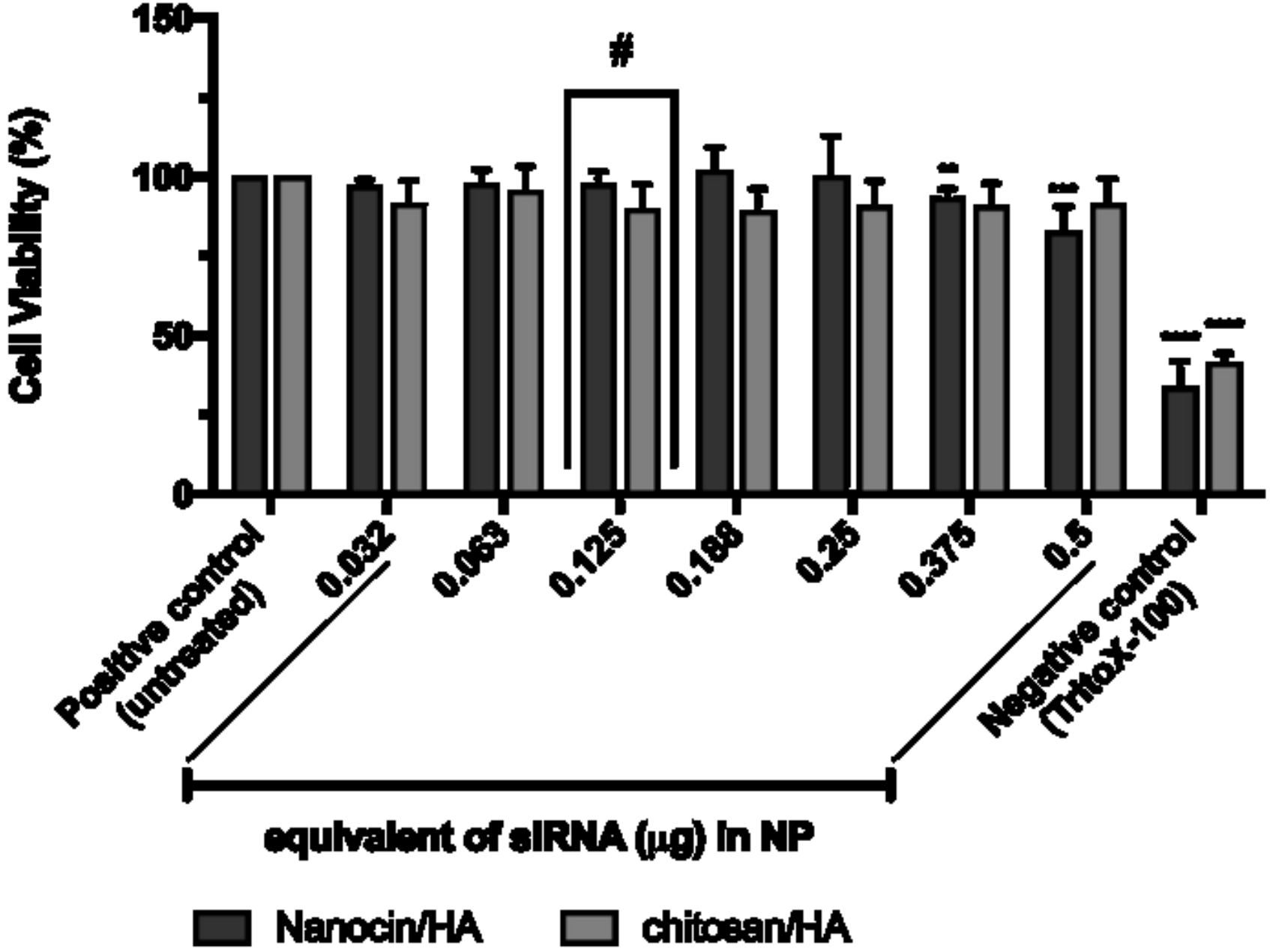
Cell Viability (%)
150
100
50
0
#
**
***
***
***
Positive control (untreated)
0.032
0.063
0.125
0.188
0.25
0.375
0.5
Negative control (TritoX-100)
equivalent of siRNA (μg) in NP
Nanocin/HA
chitosan/HA

Figure SI6

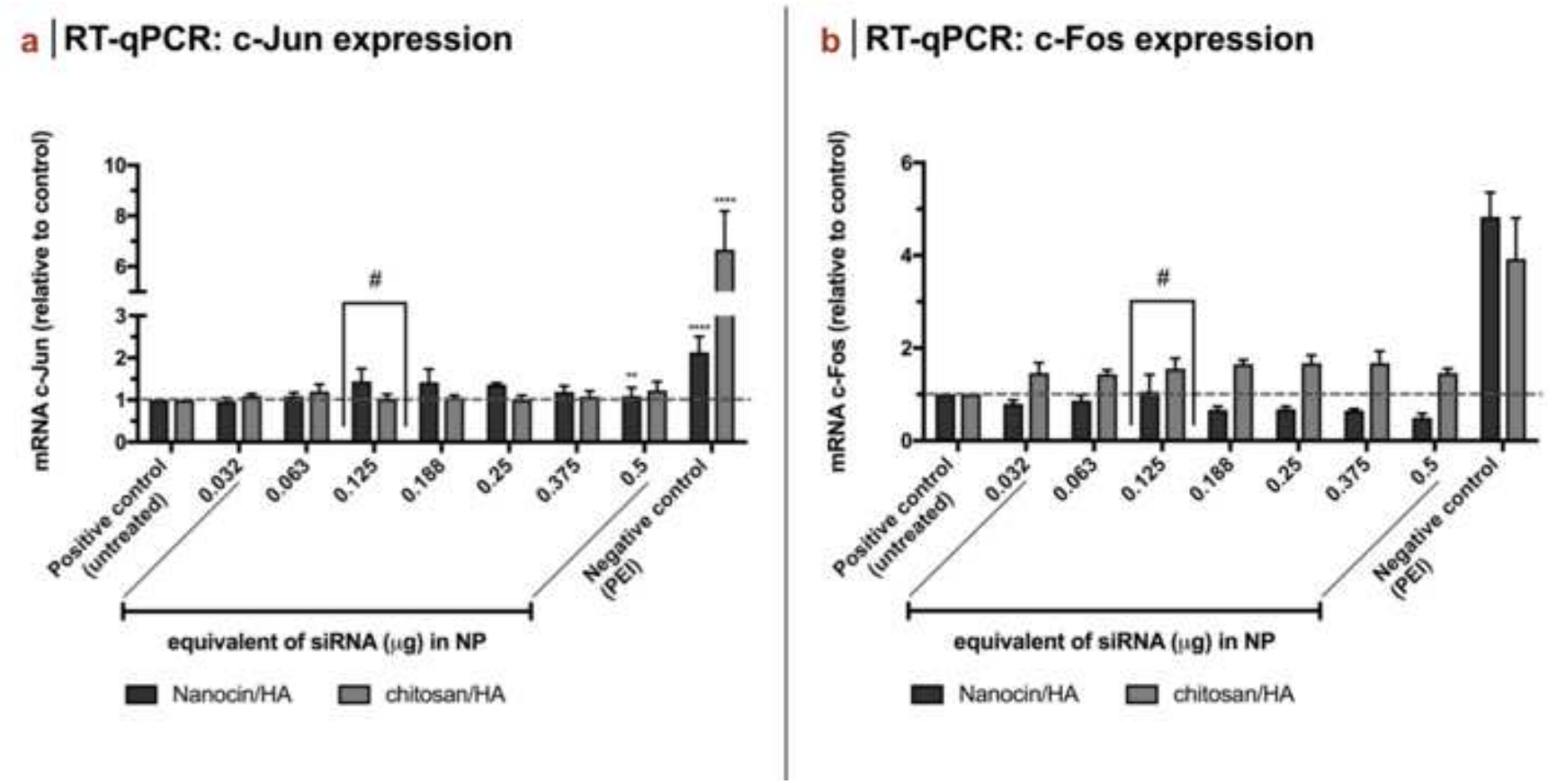
a | RT-qPCR: c-Jun expression
mRNA c-Jun (relative to control)
10
8
6
3
2
1
0
#
**
****
****
Positive control (untreated)
0.032
0.063
0.125
0.188
0.25
0.375
0.5
Negative control (PEI)
equivalent of siRNA (μg) in NP
Nanocin/HA
chitosan/HA
b | RT-qPCR: c-Fos expression
mRNA c-Fos (relative to control)
6
4
2
0
#
Positive control (untreated)
0.032
0.063
0.125
0.188
0.25
0.375
0.5
Negative control (PEI)
equivalent of siRNA (μg) in NP
Nanocin/HA
chitosan/HA